Influence of Charging Oil Condition on Torque Converter Cavitation Characteristics

Cheng Liu (liucheng@bit.edu.cn)
https://orcid.org/0000-0002-8264-5747
Meng GUO
Beijing Institute of Technology
Qingdong Yan
Beijing Institute of Technology
Wei Wei
Beijing Institute of Technology

Original Article

Keywords: Torque converter, Cavitation, CFD, Transient flow

Posted Date: May 14th, 2020

DOI: https://doi.org/10.21203/rs.3.rs-27455/v1

Title page

Influence of Charging Oil Condition on Torque Converter Cavitation Characteristics

Cheng Liu, born in 1986, is currently an assistant professor at *Beijing Institute of Technology*, *China*. He received his PhD degree from *Beijing Institute of Technology*, *China*, in 2015. His research interests include vehicle hybrid technology, fluid transmission and control, transient cavitation and control.
E-mail: liucheng@bit.edu.cn

Meng Guo, born in 1991, is currently a PhD candidate at *School of Mechanical Engineering*, *Beijing Institute of Technology*, *China*. He received his master degree from *Yanshan University*, *China*, in 2018. His research interests include fluid transmission and control, transient cavitation and fluid-structure interaction.
E-mail: guomeng826025@163.com

Qingdong Yan, born in 1964, is currently a professor at *Beijing Institute of Technology*, *China*. He received his PhD degree from *Beijing Institute of Technology*, *China*, in 1995. His research interests include Vehicle system integration technology, vehicle transmission and control technology, fluid machinery and CFD.
E-mail: yanqd@bit.edu.cn

Wei Wei, born in 1978, is currently an associate professor at *Beijing Institute of Technology*, *China*. He received his PhD degree from *Beijing Institute of Technology*, *China*, in 1995. His research interests include Modern design method of vehicle transmission system, theory and technology of vehicle automatic transmission system, design theory and test of hydraulic components.
E-mail: weiweibit@bit.edu.cn

Corresponding author：Cheng Liu　E-mail：liucheng@bit.edu.cn

ORIGINAL ARTICLE

Influence of Charging Oil Condition on Torque Converter Cavitation Characteristics

Cheng Liu[1, 2] • Meng Guo[2] • Qingdong Yan[1, 2] • Wei Wei[1, 2]

Received June xx, 202x; revised February xx, 202x; accepted March xx, 202x

Abstract: Cavitation inside a torque converter induces noise, vibration and even failure, and these effects have been disregarded in previous torque converter design processes. However, modern high-capacity torque converter applications require attention to this issue. Therefore, this study investigated the cavitation effect on a torque converter using both numerical and experimental methods with an emphasis on the influence of the charging oil feed location and charge pressure. Computational fluid dynamics (CFD) models were established to simulate the transient cavitation behaviour in the torque converter using different charging oil pressures and inlet arrangements and testing against a base case to validate the results. The CFD results suggested that cavitating bubbles mainly takes place in the stator of the torque converter. The transient cavitation CFD model yielded good aggrement with the experimental data, with an error of 7.6% in the capacity constant and 7.4% in the torque ratio. Both the experimental and numerical studies showed that cavitation induced severe capacity degradation, and that the charge pressure and charging oil configuration significantly affects both the overall hydrodynamic performance and the fluid behaviour inside the torque converter because of cavitation. Increasing the charge pressure and charging the oil from the turbine-stator clearance were found to suppress cavitation development and reduce performance degradation, especially in terms of the capacity constant. This study revealed the fluid field mechanism behind the influence of charging oil conditions on torque converter cavitation behaviour, providing practical guidelines for suppressing cavitation in torque converter.

Keywords: Torque converter • Cavitation • CFD • Transient flow

✉ Cheng Liu
liucheng@bit.edu.cn

[1] National Key Lab of Vehicular Transmission, Beijing Institute of Technology, Beijing 100081, China

[2] School of Mechanical Engineering, Beijing Institute of Technology, Beijing 100081, China

1 Introduction

A torque converter transfers rotating power through the interaction of the fluid and the cascades. Torque converters can provide continuous speed and torque ratios, moreover, it can produce effective damping to protect the transmission system from torsional vibration, thus it is extensively used in automatic transmissions and other hydraulic transmission systems. A typical automotive torque converter includes three wheels: the pump, which is driven by the engine and energises the fluid; the turbine, which discharges the fluid and drives the transmission; and the stator, which is fixed to a one-way clutch (Figure 1). These three components operate in close proximity to one another and form a circuit, with the working media cycling through the pump, turbine, and stator. The one-way clutch allows the stator to rotate freely to improve efficiency, and the lock-up clutch further increases the efficiency to nearly one by locking the pump and the turbine.

Automatic transmissions have recently been trending towards increased power density to reduce fuel consumption, leading to greater demand for smaller torque converters with higher capacity [1]. These trends require higher flow velocity in the torque converter, which leads to lower local pressures and thus greater cavitation risk. Cavitation has plagued fluid machinery for centuries [2][3], degrading performance and introducing noise, vibration, and even failure depending on the cavitation degree [4]. Considerable research effort has been devoted to understanding the cavitation mechanism to enable suppression of its effectys [5][6][7]. Cavitation in torque

converters has been reported decades ago [8][9], and continuous efforts have been put into the investigation and control of cavitation in torque converters [10].

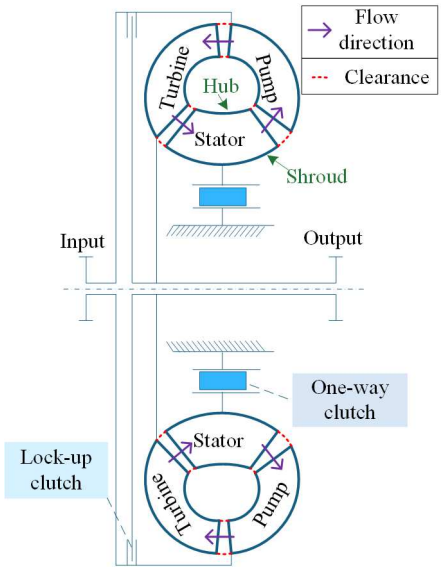

Figure 1 Schematic diagram for a typical automotive torque converter

One team conducted extensive experimental studies on torque converter cavitation. The microwave telemetry technique [11]and the nearfield acoustic test approach [12]were proposed to investigate cavitation phenomena in a series of torque converters. In another approach, Robinette et al. tested a matrix of torque converters and developed a dimensionless model for predicting cavitation [13]. Reynolds measured the sound power level in torque converters over various speed ratios and developed a response surface model to estimate the sound power of a working torque converters [14]. Watanabe et al used transparent elements to visualize the generation and collapsing of cavitating bubbles in a torque converter at the stall and captured cavitation phenomena inside the stator over various pump speeds, concluding that cavitation may be responsible for high frequency torque vibrations [15].

Because cavitation is inherently transient and small in scale, significant computing power is required for precise prediction of cavitation in torque converters. Although computational fluid dynamics (CFD) models has been extensively and effectively used in real-world case, only recently has numerical research been reported on torque converter cavitation. Ju et al. investigated the cavitation phenomena in an automotive torque converter over various speed ratios using a periodic steady-state CFD model. It was reported that cavitation mainly took place in the stator and severely degraded torque capacity [16]. Tsutsumi et al. also established a periodic steady-state CFD model to study the influence of cavitation on torque converter hydrodynamic performance [17] and concluded that stator was prone to cavitation at lower speed ratios, whereas the flow in the pump would cavitate at higher speed ratios when ambient pressure was further reduced. Liu et al. revealed the influence of the blade profile on torque converter cavitation behaviour using a fixed turbine-stator steady-state CFD model, and then improved performance by redesigning the turbine blade to reduce cavitation [18]. The team then studied the effect of the stator blade geometry on the cavitation characteristics with a periodic steady-state CFD model. It was found that the stator blade count, leaning angle, and blade nose shape significantly affected the torque capacity loss, cavitation range, and cavitation degree [19]. The team also proposed a cavitation suppression technique by cutting a slot on the stator blades. A full three-dimensional cavitation model was built to evaluate the transient cavitation behaviour over different slot configurations, and the results showed that the addition of a slot on the stator blade can suppress the cavitation degree [20].

Most of the previous research on this topic focused either on cavitation-induced issues such as performance degradation, noise, and vibration, or on empirical design models for cavitation control. However, little is known about the influence of charging oil conditions on cavitation characteristics. In general, the effects of cavitation have been disregarded in past torque converter design processes, and modern high-capacity torque converter applications require greater attention to this issue. Therefore, the study presented here used CFD modelling to investigate the influence of charging oil pressure and inlet configuration on transient cavitation characteristics. The full flow passage geometry was extracted from a base torque converter model and a refined mesh was adopted to capture transient cavitating flows. Different CFD models were developed in ANSYS CFX™ to predict the torque converter fluid behaviour based on Reynolds-averaged Navier-Stokes equations. The Rayleigh-Plesset model was implemented to capture the formation and collapse of cavity bubbles inside the torque converter. Because the cavitating flows varied greatly in scale with different charging conditions, and because the working medium flowed in a closed-loop, the CFD calculation was slow to converge. Non-cavitation, cavitation, steady-state and transient models were performed in sequence using previous results as initial conditions to improve convergence. CFD simulations with different charging oil pressures and inlet arrangements were carried out to study

the influence of charging oil conditions on the cavitation characteristics. The base model torque converter was tested under different charging conditions to validate the numerical results. Thus, this study revealed the influence of charging conditions on the transient cavitating flows inside a torque converter and provides practical guidelines to suppressing cavitation in a torque converter by controlling the charge pressure and optimizing the charging oil inlet configuration.

2 Methodology

2.1 Geometry model

The base model was a die cast converter with a high power density, as is used in off-road vehicles. The model's torus diameter was 400 mm; the blade cascades are depicted in Figure 2.

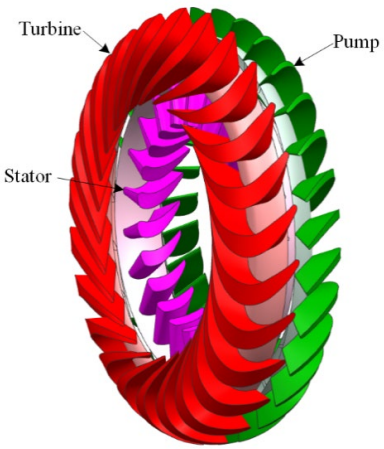

Figure 2 D400 torque converter blade cascade

In this model, the pump blade is highly twisted and the stator blade is relatively short, leading to a high mass flow rate and high power capacity. The three components are very close to each other, with a minimum clearance of 3 mm, and the heat produced inside the torque converter can be removed by supplying oil through the clearances between adjacent components, referred to as the pump-turbine clearance (P-T clearance), the turbine-stator clearance (T-S clearance), and the stator-pump clearance (S-P clearance). In real applications, this torque converter supplies oil through the S-P clearance and the charge pressure was 0.6 MPa.

2.2 CFD models

Previous research reported that cavitating bubbles mainly occurred in the stator and that the stall operating condition was the worst-case scenario. Thus, this study focused on the transient cavitation behaviour at stall, when both the stator and the turbine are stationary. Therefore, a turbine-stator fixed model was employed to simplify the CFD calculation. The leakage between different components and compressibility of the working medium were ignored, and the fluid was considered isothermal.

The three components were distributed into two domains: the rotating pump domain and the stationary turbine-stator domain. This simplification eliminated the interface between the stator and the turbine, reducing the demand on computer resources and improving convergence. The clearance between adjacent domains on the shroud was extracted as illustrated in Figure 3. An opening boundary was applied on the selected clearance to simulate different charging oil conditions.

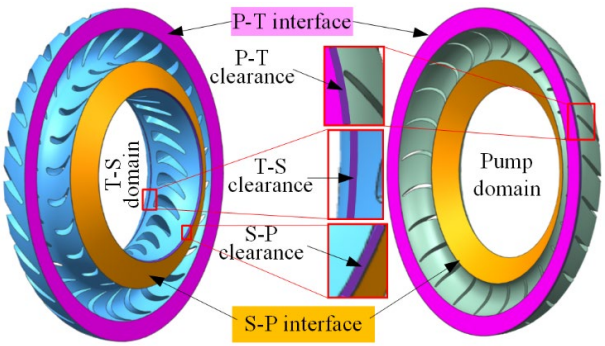

Figure 3 Full 3D fluid domains and boundaries

The pump rotated at 2000 rpm, and the turbine-stator domain was fixed to stationary, in accordance with the test condition. A non-cavitation steady-state calculation was run first, followed by a cavitation steady-state CFD simulation based on the non-cavitation results. Lastly, a transient CFD calculation with cavitation was fulfilled using the steady-state cavitation outcome as the initial condition.

2.2.1 Non-cavitation CFD model

The inherently unsteady flows and, the closed-loop configuration both deteriorate the convergence of the cavitation calculation; therefore, the non-cavitation CFD simulation was performed to provide a reasonable initial condition for the cavitation calculation. The detailed non-cavitation CFD settings are listed in Table 1.

Due to the existence of highly turbulent flow and strong reverse pressure gradient, a sophisticated turbulence model is needed to accurately simulate the turbulent flow behaviour. The shear stress transport (SST) model is a robust two-equation eddy-viscosity turbulence model that can simulate the flow turbulence by a combination of k-ω

model and k-ε model. Therefore, the SST model was employed to accurately capture the wall bounded turbulent flow. The frozen rotor interface model was applied to transfer the fluid properties between different components, and no-slip smooth walls were applied on all other boundaries except the opening.

Table 1 Non-cavitation CFD settings

Analysis type	Steady-state
Fluid properties	ρ_l=830 kg m^{-3}, μ_l=9e-3 Pa s
Turbulence model	Shear stress transport (SST)
Advection scheme	High resolution
Convergence target	RMS 1e-6
Interface model	Frozen rotor
Boundary details	No slip and smooth wall

2.2.2 Cavitation CFD model

A steady-state model considering cavitation was established to provide appropriate initial results, and then a transient cavitation CFD simulation was carried out to capture the dynamic cavitation behaviour. A vapour was added into the CFD model, and the Rayleigh-Plesset equation was implemented to govern the mass transfer between the non-condensable liquid phase and the gas phase:

$$\frac{\partial}{\partial t}\left(f_l\rho_l\right)+\frac{\partial}{\partial x_j}\left(f_l\rho_l v_j\right)=\dot{m} \tag{1}$$

By ignoring the interphase slip and heat transfer, the growth of a spherical vapour bubble can be modelled by the simplified Rayleigh-Plesset equation [21]

$$\frac{dR_B}{dt}=\sqrt{\frac{2}{3}\frac{p_v-p}{\rho_l}} \tag{2}$$

The mass transfer rate during vapourization can then be written as

$$\dot{m}=\frac{3f_v\rho_v}{R_B}\sqrt{\frac{2}{3}\frac{p_v-p}{\rho_l}} \tag{3}$$

Given that the vapourization process is much faster than the condensation process, different equations are used to govern the two processes:

$$\begin{cases}\dot{m}^- = -F_{vap}\dfrac{3f_{nuc}\left(1-f_v\right)\rho_v}{R_B}\sqrt{\dfrac{2}{3}\dfrac{p_v-p}{\rho_l}}\\ \dot{m}^+ = F_{cond}\dfrac{3f_v\rho_v}{R_B}\sqrt{\dfrac{2}{3}\dfrac{p-p_v}{\rho_l}}\end{cases} \tag{4}$$

The detailed model settings and the empirical coefficients for the vapourization ($\dot{m}^-$) and condensation ($\dot{m}^+$) are reported in Table 2.

Table 2 Cavitation CFD settings

Analysis type	Steady-state/ Transient
Vapour properties	ρ_v=2.1 kg m^{-3}, μ_v=1.2e-5 Pa s
Saturation pressure	110 Pa
Volume fraction of the nucleation site	5e-4
Initial bubble radius	1e-6 m
Convergence target	RMS 1e-5
Interface model	Frozen rotor/ Transient rotor-stator
Time step	1e-4 s
Charging oil inlet	Opening boundary
F_{vap}	50
F_{cond}	0.01
f_{nuc}	5e-4
R_B	1e-6m

Because the computing cost of capturing the interphase boundaries would be prohibitive, a homogeneous state was utilized for simplification. By assuming that the gas and the liquid phases have the same velocity and turbulence, the mixture of the two phases can be considered homogeneous and the density and dynamic viscosity can be determined by the vapour volume fraction.

Although most of the cavitation CFD settings were the same as the non-cavitation model, the convergence target was relaxed to 1e-5 for the cavitation model because the huge mixture density gradient deteriorated the convergence of the solution. The overall performance, such as component torques, were checked after the simulation to make sure they converged sufficiently. Furthermore, the steady-state cavitation model that provided the initial data for the transient calculation proved to improve the convergence effectively. Because the fluid domain of the torque converter is a closed loop (Figure 1), there is no inlet or outlet, and therefore the opening boundary was imposed on the charging oil inlet with a given static pressure. An appropriate time step was determined to capture the transient flow behaviour during one pump-turbine flow passage interaction in ten steps.

$$\Delta t=\frac{2\pi}{\omega_P-\omega_T}\cdot\frac{1}{Z_P}\cdot\frac{1}{10}=1.2e-4s \tag{5}$$

The time step was taken as 1e-4s. A total of 300 time steps were calculated, during which the pump completed at least one revolution.

2.3 Experimental setup

A torque converter dynamometer test cell was built to test the torque converter (Figure 4). The experimental setup consisted of a diesel engine, hydraulic supply system, test fixture, torque/speed sensors and absorbing dynamometer. A 588-kW diesel engine was used to drive the test rig, and

a 1200-kW electric dynamometer was mounted to simulate the load. The hydraulic supply system allowed control of the oil temperature and the charge pressure imposed upon the torque converter. The engine speed, i.e. the pump rotating speed, was stabilized at 2000 rpm throughout the test, and the turbine was held stationary by the motor to simulate the stall operating condition. The pump torque and the turbine torque were collected by torque sensors. The capacity constant (C) and the torque ratio (TR) could then be calculated as follows:

$$\begin{cases} C = \dfrac{T_P}{\omega_P^2 D^5} \\ TR = \dfrac{T_T}{T_P} \end{cases} \tag{6}$$

The charge pressure was varied across three levels - 0.3, 0.6 and 0.9 MPa - during the test to evaluate the influence of charge pressure on the torque converter's overall hydrodynamic performance. The oil temperature was regulated at 90 ℃ and the oil was supplied from different locations to evaluate the influence of oil feed location on hydrodynamic performance.

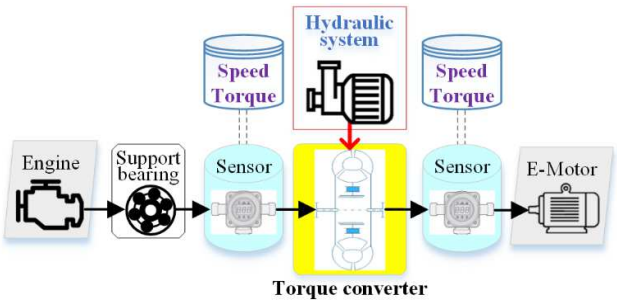

Figure 4 The schematic diagram of torque converter test cell

3 Results

3.1 CFD model validation

Figure 5 shows the results of the grid independence study that was performed on the steady-state CFD model to determine an appropriate grid density, and the torques derived from different mesh size models are listed in Table 3. It was found that 16 million elements would yield stable results. The mesh around the blades was further refined with a 12-layer prism grid to reduce the average y+ value to less than two [22], enabling a low-Re formulation of the SST model for precise near-wall flow predictions.

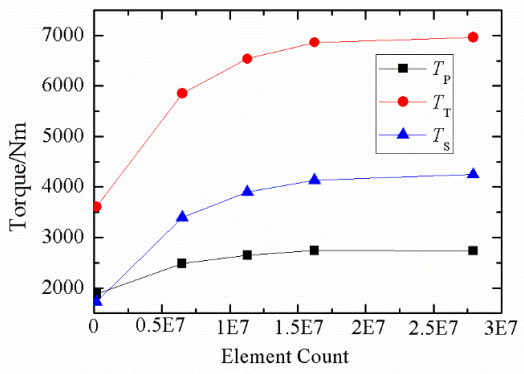

Figure 5 Predicted torque results under variant element density

Table 3 Grid independence study results

Mesh Size/m	Tot. elements	Pump torque		Turbine torque		Stator torque	
		T_P/Nm	Div./%	T_T/Nm	Div./%	T_S/Nm	Div./%
0.06	164243	1877	32.6	3607	62.3	1729	96.3
0.0045	6489097	2489	6.6	5853	11.7	3394	15.0
0.0025	11279385	2653	3.4	6536	5.0	3903	5.9
0.0019	16228786	2743	-0.3	6862	1.5	4135	2.7
0.0014	27921225	2735	–	6966	–	4246	–

The 0.6 MPa charge pressure and S-P charging oil position were the conditions used to validate the CFD model. Table 4 compares the CFD results to the experimental data, showing that all of the CFD models overestimated the hydrodynamic performance. The non-cavitation CFD model, exhibited the largest deviation at stall operating condition, overestimating the capacity constant and the torque ratio by 33.4% and 15.2%, respectively. The corresponding deviations in the steady-state cavitation CFD model were 9.2% and 10.6% , and the transient cavitation model further reduced the prediction error to within 7.6% for both performance indices, indicating that the transient cavitation CFD model can predict the overall hydrodynamic performance with acceptable accuracy. Furthermore, the comparison between the non-cavitation CFD model and the cavitation CFD model confirmed that the torque converter suffered from heavy cavitation, and the differences in the deviations of the two models indicated the cavitation degree.

Table 4 CFD predictions versus test data

	C/kg rad^{-2} m^{-3}	*C-error*	TR/Nm	*TR-error*
Test data	4.58	–	2.17	–
Non-cavitation	6.11	33.4	2.50	15.2
Steady-state cavitation	5.00	9.2	2.40	10.6
Transient cavitation	4.93	7.6	2.33	7.4

3.2 Effect of charging oil configuration

The effect of the feed oil location was studied by applying

the opening boundary condition with 0.6 MPa static pressure upon three different clearances. The results are listed in Table 5.

Table 5 Transient CFD predictions of hydrodynamic performance with different charging oil inlet configurations

Oil inlet	T_P/Nm	T_T/Nm	T_S/Nm	C/ kg rad^{-2} m^{-3}	TR/Nm
P-T clearance	1840.8	4460.8	2584.7	4.10	2.42
T-S clearance	2273.1	5387.1	3105.7	5.07	2.37
S-P clearance	2212.3	5149	2937	4.93	2.33

Table 5 shows that when the charging oil was supplied at the P-T clearance, the capacity constant was significantly lower and the torque ratio was slightly higher than when the oil was supplied at the other two clearances. Furthermore, when the oil was supplied from the stator inlet (T-S clearance), the capacity constant and the torque ratio were slightly higher than when the oil was supplied from the stator outlet (S-P clearance). These results suggest that the best method of supplying charging oil to the torque converter is at the T-S clearance, which showed less cavitation than the other two charging configurations.

3.3 Effect of charge pressure

The effect of charge pressure was studied by varying the charge pressure imposed upon the S-P clearance at three different levels: 0.3, 0.6, and 0.9 MPa. The simulation results are reported in Table 6.

Table 6 Torque converter performance over variant charge pressure

Charge pressure	CFD model	T_P/Nm	T_T/Nm	C/ kg rad^{-2} m^{-3}	TR/Nm
0.3 MPa	Non-cavitation	2741	6858	6.11	2.50
	cavitation	1983.7	4512.9	4.42	2.27
0.6 MPa	Non-cavitation	2743	6861.7	6.11	2.50
	cavitation	2212.3	5149	4.93	2.33
0.9 MPa	Non-cavitation	2746	6865.1	6.12	2.50
	cavitation	2477.8	5874	5.52	2.37

Table 6 shows that the charge pressure change did not affect the hydrodynamic performance for the non-cavitation simulations because the non-cavitation model only solved the incompressible fluid phase. However, the cavitation results indicated that increased charge pressure significantly improved the performance, implying that cavitation could be suppressed by increasing the charge pressure.

4 Discussion

The base case, with a charge pressure of 0.6 MPa and oil fed through the S-P clearance, was analysed to explore the transient cavitation behaviour in the torque converter. The CFD results indicated that cavitation in the base model brings about severe torque capacity loss. Table 4 shows that the torque converter suffered a reduction of 19.3% in the capacity constant. The cavitation bubbles blocked the main flow inside the torque converter, reducing the mass flow rate (Figure 6 - Figure 8). The capacity of the torque converter is an indicator of power-absorbing ability, and a higher mass flow rate generally leads to higher capacity. Cavitation seriously degrades capacity when the bubbles block the main flow. The model showed that most of the vapour was generated at the stator nose on the suction side, and attached cavities can be found at the turbine nose (Figure 6).

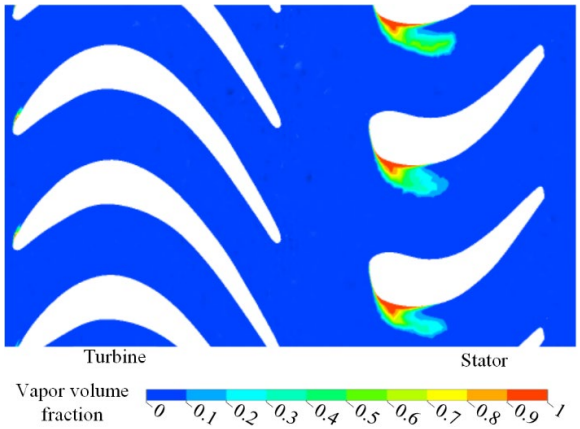

Figure 6 Vapour volume fraction distribution at the final time step for the base case.

Although no measurable cavitation occurred in the pump domain, isolated cavitation bubbles that originated from cavity shedding in the stator domain were found in the pump domain (Figure 6, Figure 7). As the fluid exiting the pump struck the turbine cascade with a large incidence angle, small-scale attached cavities were generated at the turbine blade nose near the suction side (Figure 7). Cavitation was observed in the stator and the turbine domain. The cavities covered almost the entire stator nose, with scattered bubbles that detached from the stator domain entering the pump domain. However, these scattered bubbles collapsed soon after travelling to the latter part of the pump flow passage because of the high local pressure.

Figure 8 demonstrates that the oil velocity was relatively uniform for the non-cavitation case. Only a minor secondary flow region was found at the pump blade tail on the suction side. However, when cavitation was considered,

much vapour was generated in the stator domain, leading to severe reverse flows in all three components. These reverse flows, along with the bubble blockage, significantly reduced the mass flow rate inside the torque converter, and consequently resulted in capacity loss.

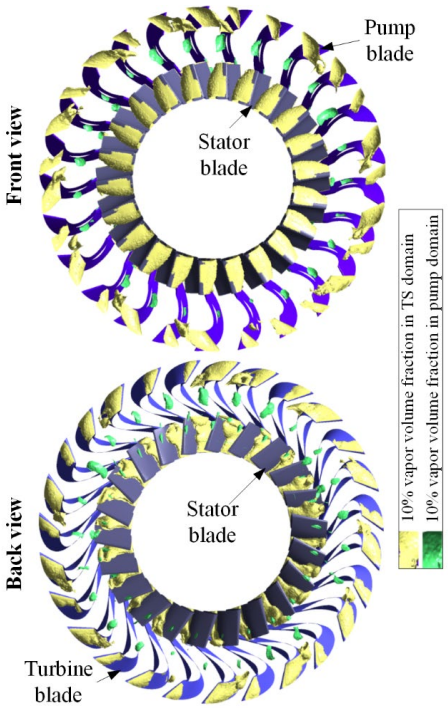

Figure 7 10% vapour volume fraction distribution in front view (looking at the stator leading edge) and back view (looking at the stator trailing edge)

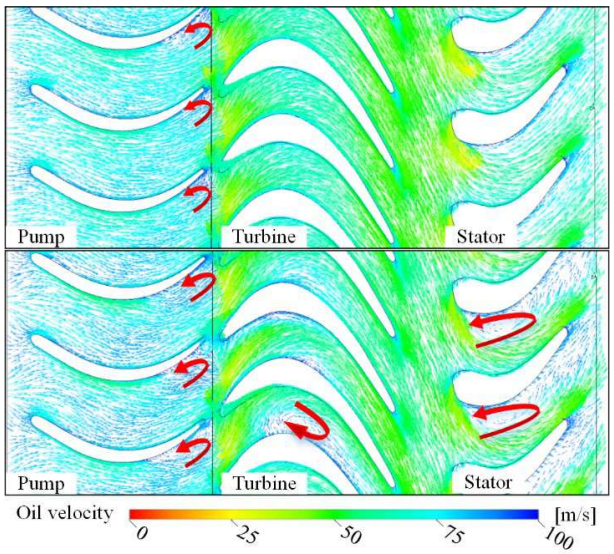

Figure 8 The oil velocity distribution derived from non-cavitation simulation (upper) and transient cavitation simulation at the final time step (lower). The reverse flow is indicated by arrow.

The cavitation process inside the stator domain for the base case consisted of two types of cavitation: a stable sheet cavitation attached to the stator blade near the entrance and an unstable cavitation that tore part of the bubble and detached periodically. These cavitation types are shown in Figure 9, which depicts the transient cavitation behaviour inside the stator domain. Cavitation vacancies formed on the stator suction side (Figure 9 (a)) and grew towards the stator trailing edge (Figure 9 (b)). When the vacancies reached the blade mid-span, a re-entrant jet, induced by the reverse flow and enhanced by the negative pressure gradient in the corresponding area, moved upstream from the blade end to the blade nose, splitting the cavity (Figure 9 (c)). The shed cavity travelled downstream with the main flow, and the attached cavity shrank towards the blade nose (Figure 9 (d)). This shedding process repeated periodically.

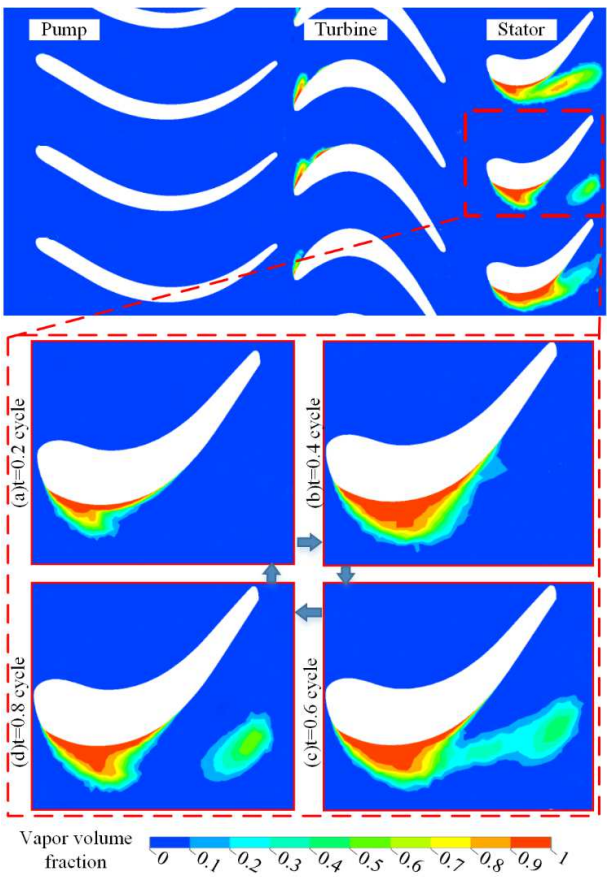

Figure 9 The transient cavitation process shown in the unfolded view

The investigation of the oil inlet position indicated that to suppress cavitation, the best location at which to supply the charging oil was the turbine-stator clearance, whereas

pump-turbine clearance resulted in the highest torque capacity degradation. Two charging oil inlet arrangements were experimentally tested, and the results are compared with numerical predictions in Table 7. The predictions agreed fairly well with the test data, and the numerical and the experimental results both indicated that supplying the oil from the T-S clearance resulted in higher capacity, i.e., less cavitation.

Table 7 The numerical and experimental torque converter stall performance over different charging oil inlet arrangements. Charge pressure = 0.6 MPa

Oil inlet		*C*/ kg rad^{-2} m^{-3}	*C-error*	*TR*/Nm	*TR-error*
T-S clearance	Test	4.75	–	2.19	–
	CFD	5.07	6.7%	2.37	8.2%
S-P clearance	Test	4.58	–	2.17	–
	CFD	4.93	7.6%	2.33	7.4%

As the generation and collapse of cavities were simulated by a homogeneous cavitation model, no interface between the two phases was calculated, and the vapour was characterized by the vapour volume fraction within the homogeneous mixture. The cavitation processes under the three different charging oil configurations were visualized using a 10% vapour volume fraction iso-surface distribution in the stator domain and the vapour volume fraction distribution in the unfolded view. The averaged absolute pressure distributions in the meridional view were also shown to illustrate the influence of the oil feed position. The cavitation region was mainly located in the front part of the stator passage in all the three cases.

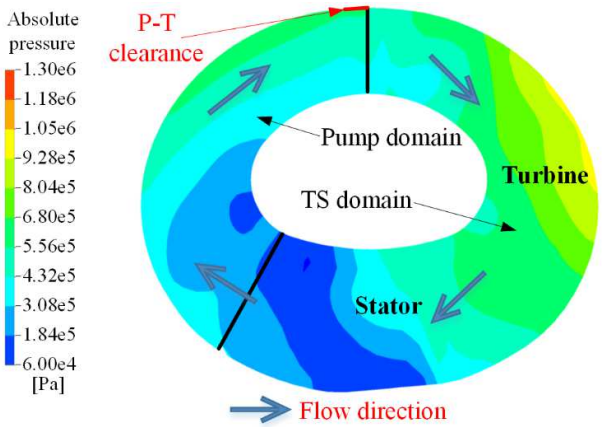

Figure 10 Meridionally averaged pressure distribution when the oil is charged from the P-T clearance. Charge pressure =0.6 MPa.

Figure 10 illustrates the meridionally averaged pressure distribution when the oil was fed through the P-T clearance with 0.6 MPa pressure. The absolute pressure in the turbine domain was clearly the highest among all components, and the stator pressure was the lowest. A significant pressure gradient can be observed in the whole fluid domain, and the large-scale low-pressure region in the stator domain gave rise to cavitation.

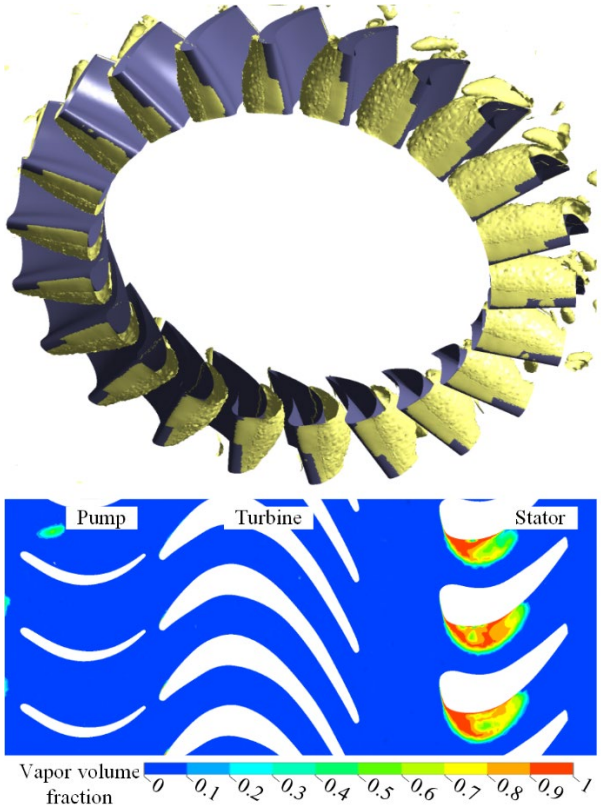

Figure 11 10% vapour volume fraction distribution (upper) and vapour volume fraction distribution in the unfolded view (lower) when the oil is charged from the P-T clearance. Charge pressure = 0.6 MPa

Figure 11 shows that when the charging oil was supplied to the torque converter through the P-T clearance, significant cavitation took place in the stator domain. The cavitation vacancies covered the entire stator nose and spread into the stator midspan. These large cavities blocked the main flow and drastically degraded capacity. No cavitation could be found in the turbine domain as a result of the high pressure of the oil supplied at the turbine inlet, which led to a relatively higher torque ratio compared to the other two cases (Table 5).

The meridionally averaged pressure for the S-P feed oil location case is depicted in Figure 12, which shows a high-pressure region in the turbine domain near the shroud. Although the pressure distribution pattern was similar to the P-T feed oil location case, the overall pressure level

was greatly increased compared to the P-T clearance case (Figure 10).

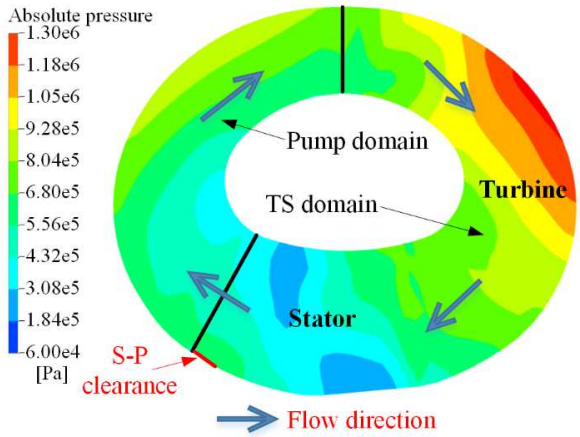

Figure 12 Meridionally averaged pressure distribution when the oil is charged from the S-P clearance. Charge pressure =0.6 MPa.

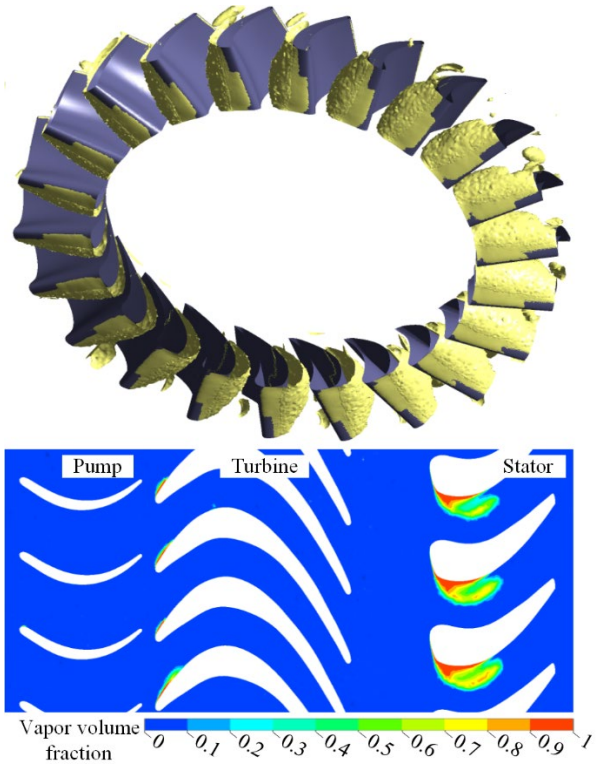

Figure 13 10% vapour volume fraction distribution (upper) and vapour volume fraction distribution in the unfolded view (lower) when the oil is charged from the S-P clearance. Charge pressure = 0.6 MPa

Figure 13 shows that when the oil was supplied from through the S-P clearance, the cavitation region shrank towards the stator blade leading edge, and consequently reduced the amount of cavitation. However, the cavities still covered almost the entire stator blade nose, and small cavities were observed in the turbine domain as the high-velocity fluid struck the turbine blade, which contributed to the torque ratio degradation.

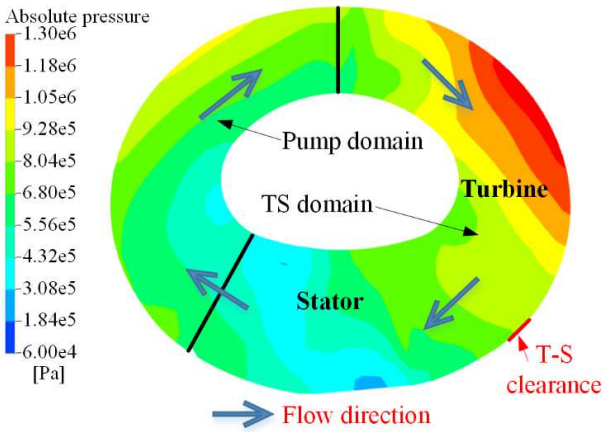

Figure 14 Meridionally averaged pressure distribution when the oil is charged from the T-S clearance. Charge pressure =0.6 MPa.

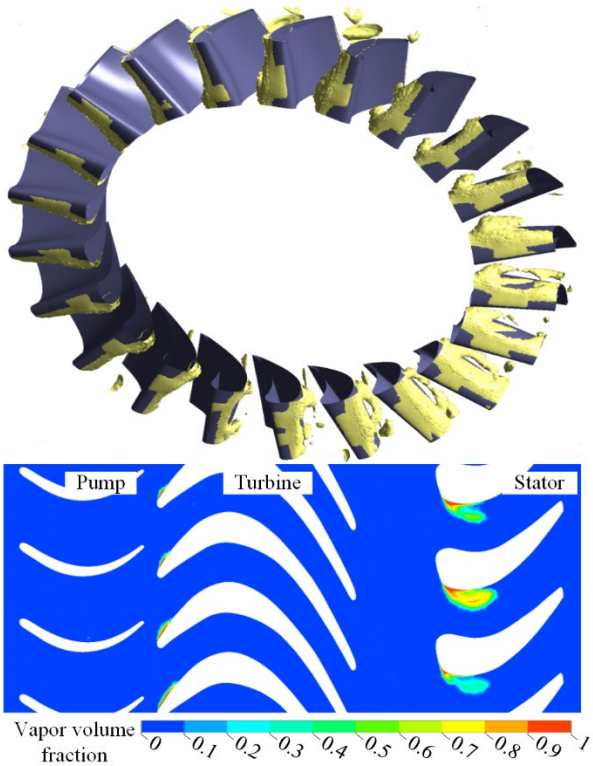

Figure 15 10% vapour volume fraction distribution (upper) and vapour volume fraction distribution in the unfolded view (lower) when the oil is charged from the T-S clearance. Charge pressure = 0.6 MPa

The averaged pressure distribution in the T-S case (Figure 12) is almost the same as that in the S-P case (Figure 14). However, as the high-pressure oil was supplied to the inlet of the stator, the overall pressure level in the stator domain was slightly higher and the low-pressure region was smaller.

Figure 15 reveals that, when the oil was supplied from the T-S clearance, the cavitation region further shrank towards the stator blade leading edge and barely covered the stator nose. Because the cavitation started at the stator nose, when high-pressure oil was supplied to the stator inlet, cavitation and the associated capacity loss were partially suppressed. However, small cavities remained in the turbine flow passages, indicating that the cavitation condition in the turbine domain was not improved in this case.

The investigation of the charge pressure effect shows that the performance degradation decreased with an increasing charge pressure. The reason for this is straightforward: higher charge pressure increases the overall pressure level inside the torque converter and suppresses the cavitation process. The numerical predictions are compared to the test data in Table 8.

Table 8 The numerical and experimental torque converter stall performance over various charge pressures. Oil is charged from the S-P clearance

Charge pressure		C/ kg rad^{-2} m^{-3}	*C-error*	*TR*/Nm	*TR-error*
0.3 MPa	Test	4.43	–	2.19	–
	CFD	4.42	-0.2%	2.27	3.7%
0.6 MPa	Test	4.58	–	2.17	–
	CFD	4.93	7.6%	2.33	7.4%
0.9 MPa	Test	4.97	–	2.18	–
	CFD	5.52	11.1%	2.37	8.7%

It is clear from both the numerical and the experimental results that the capacity constant increased as the charge pressure increased. The numerical results show that the torque ratio increased slightly with an increasing charge pressure, however, the test results prove that the charge pressure does not have a significant effect on the torque ratio.

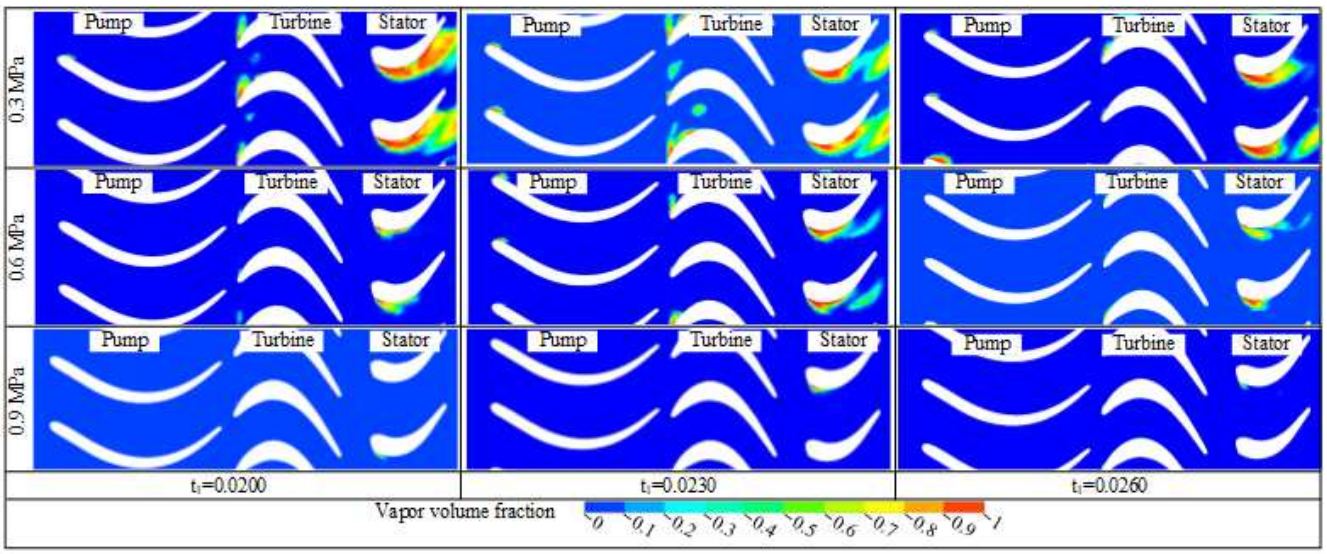

Figure 16 Vapour volume fraction distributions at different time steps over different charge pressures. The oil is supplied from the S-P clearance

The vapour volume fraction distributions shown in Figure 16 indicate that charge pressure has a significant effect on the cavitation degree and the cavitation form. The figure shows significant reduction in the cavitation region as the charge pressure increases. For all three charge pressure settings, cavitation mainly occurred in the stator domain, and all cavitation originated on the suction side of stator blade near the nose, where the flow exiting the turbine struck the stator cascade with a big incidence angle and velocity. Severe unsteady cavitation could also be found in the turbine under the 0.3 MPa charge pressure. However, only scattered small scale cavities were generated in the turbine under higher charge pressure conditions. The degree of cavitation decreased with an increasing charge pressure, leading to lower capacity degradation. It was found that the cavitation flows under 0.3MPa and 0.6 MPa were quite unsteady, particularly those flows in the stator domain. When the charge pressure was further increased to 0.9 MPa, the cavitation in the pump and the turbine domain was almost eliminated;

moreover, in the stator domain, the cavitation switched from unsteady shedding cavitation to steady attached cavitation and the cavitation region shrank drastically towards the stator nose.

The cavitation potential can be characterized by a non-dimensional cavitation number σ. When σ drops below a critical level, cavitation occurs, such that lower σ implies a higher degree of cavitation. This value is calculated as follows:

$$\sigma = \frac{p_{ref} - p_v}{0.5\rho_l v_{ref}^2} \tag{7}$$

Where p_{ref} represents the charge pressure, and v_{ref} is directly correlated to the mass flow rate, given as

$$v_{ref} = \frac{MF}{A\rho_l} \tag{8}$$

Where A is constant throughout the whole flow passage. In this model, A equalled to 2.7e-2 m^2.

The cavitation numbers for all the cases are shown in Table 9 and Figure 17. These results indicated that for a given charge oil inlet configuration, the cavitation number corresponded to the cavitation potential. The cavitation number decreased along with the charge pressure, resulting in more cavitation. However, cavitation number is not useful for assessing cavitation degree among different charge oil configurations. For instance, although the cavitation number for the P-T clearance case ranked the highest among all calculated samples (Figure 17), this case suffered from severe cavitation. The P-T clearance was located at the largest radius of the torus (Figure 1), and the pressure dropped significantly with a decreasing torus radius as a result of decreased centrifugal pressure (Figure 10). However, cavitation mainly occurred inside the stator domain, which had the lowest torus radius among all three components. Contrary to those results, the cavitation number for the T-S clearance case was slightly lower than that of the S-P clearance, even though the cavitation degree in the T-S clearance case was lower than that in the S-P clearance because high-pressure oil was supplied near the cavitation region.

Table 9 Cavitation numbers under various charging conditions

Charging position	Charge pressure	Mass flow rate	Cavitation number
S-P clearance	0.3 MPa	330.8 kg s^{-1}	3.343
S-P clearance	0.6 MPa	386.1 kg s^{-1}	4.909
S-P clearance	0.9 MPa	407.4 kg s^{-1}	6.614
P-T clearance	0.6 MPa	311.2 kg s^{-1}	7.556
T-S clearance	0.6 MPa	390.1 kg s^{-1}	4.811

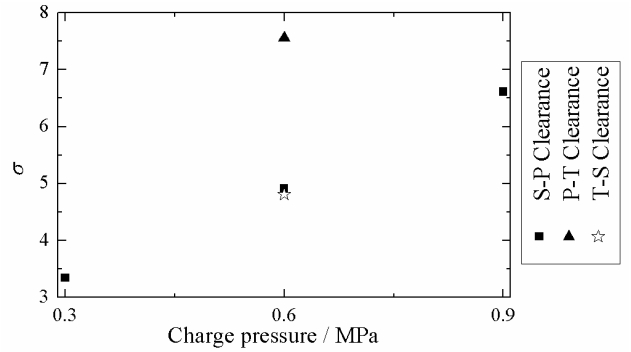

Figure 17 Cavitation numbers over various charge pressures and charge oil positions

5 Conclusion

This study investigated the transient cavitation behaviour in a torque converter at stall operating condition through a full three-dimensional CFD model. The turbine and the stator were united as one domain to simplify the simulation. The model was validated against experimental data, and the effects of the charging oil pressure and feed location were investigated.

Cavitation inside the torque converter brought about severe performance degradation, especially in terms of the torque capacity. For the base case, the non-cavitation CFD simulation overpredicted the capacity constant by 33.4% compared to the experimental results, whereas the cavitation CFD model limited the deviation to within 7.6%. The comparison between the non-cavitation and the cavitation calculations could be used to determine the cavitation degree, and thereby provide engineers with useful tools for the consideration of cavitation. The charging oil feed location had a significant effect on the cavitation characteristics inside the torque converter. Supplying the oil from the P-T clearance led to lower pressure inside the stator domain and consequently resulted in heavy cavitation. The charging oil feed location in terms of cavitation suppression was the T-S clearance, i.e., the stator inlet. Because cavitation mainly originated at the stator nose, supplying high-pressure oil to the stator inlet raised the average local pressure at the corresponding area and thus suppressed cavitation.

The charge pressure also significantly influenced the cavitation degree at the stall operating condition. The numerical and experimental studies both revealed that higher charge pressures increased the overall pressure level inside the torque converter and consequently suppressed cavitation. The transient CFD model revealed that cavities periodically shed in both the turbine and stator domains when the charge pressure was insufficient. Increasing the

charge pressure first eliminated the cavitation bubbles in the turbine and pump domains, and further increases in charge pressure led to cavitation suppression in the stator domain.

The proposed CFD model agreed fairly well with the experimental results; however, this study addressed only the influence of cavitation on external hydrodynamic performance. Cavitation bubble visualization and more sophisticated measurements, such as internal pressure, noise, and vibration tests, would be required to validate the cavitating flow behaviour. Furthermore, the numerical error increased with an increasing charge pressure, mainly because of the inconsistency between the CFD boundary settings and the test conditions. In order to improve the simulation accuracy, internal fluid flow measurements are necessary. The pressure level can be measured via micro-scale pressure sensors, and the measured pressure can be imposed upon the CFD boundary to increase the model fidelity. This will be a subject of future work.

6 Declaration

Funding

Supported by National Natural Science Foundation of China (NSFC) through Grant No. 51475041 and 51805027, Beijing Institute of Technology Research Fund Program for young Scholars (3030011181804) and Vehicular Transmission Key Laboratory Fund.

Availability of data and materials

The datasets supporting the conclusions of this article are included within the article.

Authors' contributions

The author' contributions are as follows: Cheng Liu performed the data analyses, designed and performed the experiments, and wrote the manuscript; Meng Guo contributed significantly to analysis and manuscript preparation; Qingdong Yan contributed to the conception of the study; Wei Wei and Houston G. Wood helped perform the analysis with constructive discussions.

Competing interests

The authors declare no competing financial interests.

Consent for publication

Ethics approval and consent to participate

Nomenclature

f_l	Liquid volume fraction
ρ_l	Liquid density / kg m^{-3}
v_j	Velocity / m s^{-1}
$\dot{m}$	Interphase mass transfer per unit / kg s^{-1}
R_B	Bubble radius, m
p_v	Vapour pressure / Pa
p	Local pressure / Pa
f_v	Vapour volume fraction
ρ_v	Vapour density / kg m^{-3}
f_{nuc}	Volume fraction of the nucleation site
F_{vap}	Vapourization constant
F_{cond}	Condensation constant
T_{P}	Pump torque / N m
T_{T}	Turbine torque / N m
T_{S}	Stator torque / N m
C	Capacity constant / kg rad^{-2} m^{-3}
ω_{P}	Pump rotating speed / rad s^{-1}
ω_{T}	Turbine rotating speed / rad s^{-1}
Z_P	Pump blade count
D	Torque converter torus diameter / m
TR	Torque ratio
σ	Cavitation number
p_{ref}	Reference pressure / Pa
v_{ref}	Reference velocity / m s^{-1}
MF	Mass flow rate / kg s^{-1}
A	Toroidal area / m^2

References

[1] Usui, T., Okaji, T., Muramatsu, T., and Yamashita, Y. Development of a compact ultra-flat torque converter equipped with a high-performance damper. *SAE Paper*, 2015, 01(1088). DOI: 10.4271/2015-01-1088

[2] Chen, Q. P., Wu, M. M., Kang, S., Liu, Y., and Wei, J. C.. Study on cavitation phenomenon of twin-tube hydraulic shock absorber based on CFD. *Engineering Applications of Computational Fluid Mechanics*, 2019, 13(1): 1049-1062.

[3] Kobayashi, H, Hagiwara, R., Kawasaki, S., Uchiumi, M., Yada, K., and Iga, Y.. Numerical analysis of suppression effect of asymmetric slit on cavitation instabilities in cascade. *ASME J. Fluids Eng.*, 2018, 140 (2): 021302. DOI: 10.1115/1.4037989

[4] Wang, J., Wang, Y., Liu, H. L., Si, Q. R., and Dular, M.. Rotating corrected-based cavitation model for a centrifugal pump. *ASME J. Fluids Eng.*, 2018, 140 (11): 111301. DOI: 10.1115/1.4040068

[5] Geng, L. L., and Escaler, X. Assessment of RANS turbulence models and Zwart cavitation model empirical coefficients for the simulation of unsteady cloud cavitation. 2020, 14 (1): 151-167.

[6] Shim, H., Kim, K, and Choi, Y.. Three-objective optimization of a centrifugal pump to reduce flow recirculation and cavitation. *ASME J. Fluids Eng.*, 2018, 140(9): 091202. DOI: 10.1115/1.4039511

[7] Liu, X. M., Wu, Z. H., Li, B. B., Zhao, J. Y., He, J., Li, W., Zhang, C., and Xie, F. W.. Influence of inlet pressure on cavitation characteristics in regulating valve. *Engineering Applications of Computational Fluid Mechanics*, 2020, 14(1): 299-310.

[8] Marathe, B.V., and Lakshminarayana, B.. Experimental investigation of steady and unsteady flow field downstream of an automotive torque converter turbine and stator. *International Journal of Rotating Machinery*, 1995, 2(2): 67-84. DOI: 10.1155/S1023621X95000224

[9] Dong, Y., Korivi, V., Attibele, P., and Yuan, Y. . Torque converter CFD engineering part II: performance improvement through core leakage flow and cavitation control. *SAE Paper*, 2002, 01(0884). DOI: 10.4271/2002-01-0884

[10] Robinette, D.L.. Detecting and predicting the onset of cavitation in automotive torque converters. Ph.D. dissertation, Michigan Technological University, Houghton, MI. 2007.

[11] Anderson, C.L., Zeng, L., Sweger, P.O., and Narain, A.. Experimental investigation of cavitation signatures in an automotive torque converter using a microwave telemetry technique. *International journal of rotating machinery*, 2003, 9(6): 403-410. DOI: 10.1155/S1023621X03000381

[12] Walber, C., Blough, J.R., Johnson, M., and Anderson, C.. Measuring and comparing frequency response functions of torque converter turbines submerged in transmission fluid. *SAE Paper*, 2011, 01(1662). DOI: 10.4271/2011-01-1662

[13] Robinette, D.L., Schweitzer, J.M., Maddock, D.G., Anderson, C.L., Blough, J.R., and Johnson, M.A.. Predicting the onset of cavitation in automotive torque converters – part II a generalized model. *International Journal of Rotating Machinery*, 2008: 803940. DOI: 10.1155/2008/312753

[14] Reynolds, C.D.. Characterization of torque converter cavitation sound power level over varying speed ratio. Ph.D. dissertation, Michigan Technological University, Houghton, MI. 2016.

[15] Watanabe, S., Otani, R., Kunimoto, S., Hara, Y., and Yamaguchi, T.. Vibration Characteristics Due to Cavitation in Stator Element of Automotive Torque Converter at Stall Condition. *ASME Paper*, No. FEDSM2012-72418. 2012. DOI: 10.1115/FEDSM2012-72418

[16] Ju, J., Jang, J., Choi, M. and Baek, J. H.. Effects of cavitation on performance of automotive torque converter. *Advances in Mechanical Engineering*, 2016, 8(6): 1-9. DOI: 10.1177/1687814016654045

[17] Tsutsumi, K., Watanabe, S., Tsuda, S., and Yamaguchi, T.. Cavitation simulation of automotive torque converter using a homogeneous cavitation model. *European Journal of Mechanics B/Fluids*, 2017, 61(2): 263-270. DOI: 10.1016/j.euromechflu.2016.09.001

[18] Liu, C., Wei, W., Yan, Q.D., Weaver, B.K.. Torque converter capacity improvement through cavitation control by design. *ASME J. Fluids Eng.*, 2017, 139(4): 041103. DOI: 10.1115/1.4035299

[19] Liu, C., Wei, W., Yan, Q.D., Weaver, B.K., Wood, H.G.. Influence of stator blade geometry on torque converter cavitation. *ASME J. Fluids Eng.*, 2018, 140(4): 041102. DOI: 10.1115/1.4038115

[20] Liu, C., Wei, W., Yan, Q.D., Weaver, B.K., Wood, H.G.. On the application of passive flow control for cavitation suppression in torque converter stator. *International Journal of Numerical Methods for Heat & Fluid Flow*, 2019, 29(1): 204-222. DOI: 10.1108/HFF-11-2017-0473

[21] Bakir, F., Rey, R., Gerber, A.G., Belamri, T. and Hutchinson, B.. Numerical and experimental investigations of the cavitating behaviour of an inducer. *International Journal of Rotating Machinery*, 2004, 10(1): 15-25.

[22] Menter, F. R.. 2-equation eddy-viscosity turbulence models for engineering applications. *AIAA Journal*, 1994, 32(8): 1598-1605.

Biographical notes

Cheng Liu, born in 1986, is currently an assistant professor at *Beijing Institute of Technology*, *China*. He received his PhD degree from *Beijing Institute of Technology*, *China*, in 2015. His research interests include vehicle hybrid technology, fluid transmission and control, transient cavitation and control.
E-mail: liucheng@bit.edu.cn

Meng Guo, born in 1991, is currently a PhD candidate at *School of Mechanical Engineering*, *Beijing Institute of Technology*, *China*. He received his master degree from *Yanshan University*, *China*, in 2018. His research interests include fluid transmission and control, transient cavitation and fluid-structure interaction.
E-mail: guomeng826025@163.com

Qingdong Yan, born in 1964, is currently a professor at *Beijing Institute of Technology*, *China*. He received his PhD degree from *Beijing Institute of Technology*, *China*, in 1995. His research interests include Vehicle system integration technology, vehicle transmission and control technology, fluid machinery and CFD.
E-mail: yanqd@bit.edu.cn

Wei Wei, born in 1978, is currently an associate professor at *Beijing Institute of Technology*, *China*. He received his PhD degree from *Beijing Institute of Technology*, *China*, in 1995. His research interests include Modern design method of vehicle transmission system, theory and technology of vehicle automatic transmission system, design theory and test of hydraulic components.
E-mail: weiweibit@bit.edu.cn

Figures

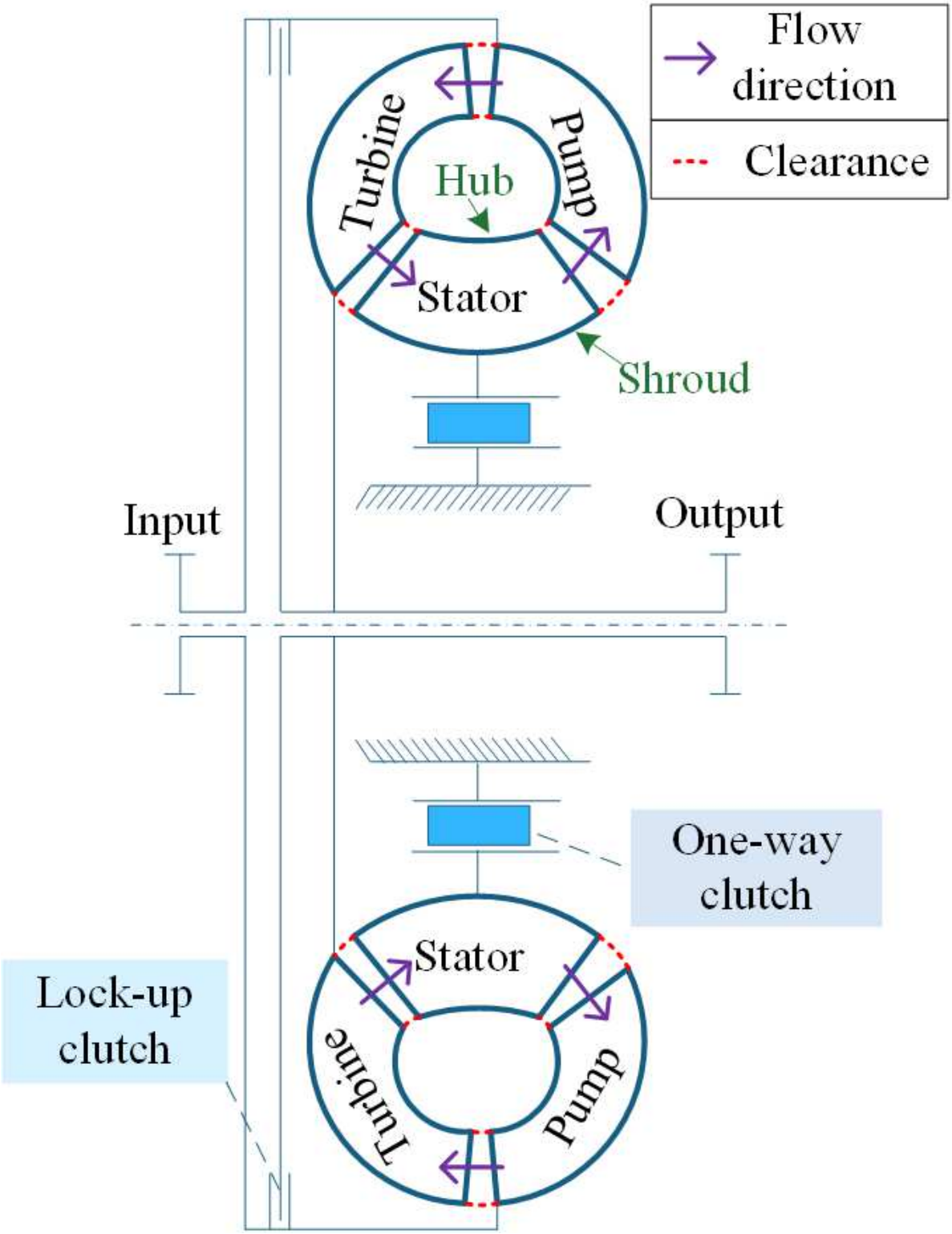

Figure 1

Schematic diagram for a typical automotive torque converter

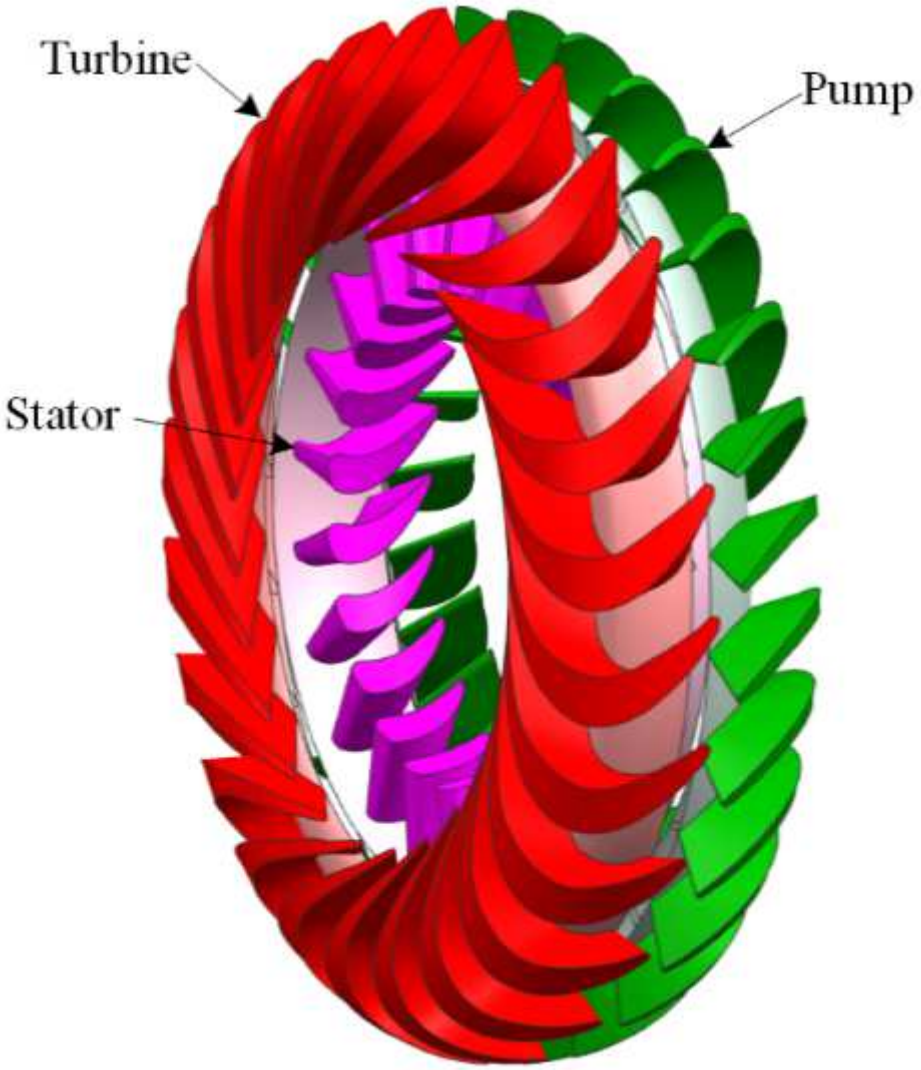

Figure 2

D400 torque converter blade cascade

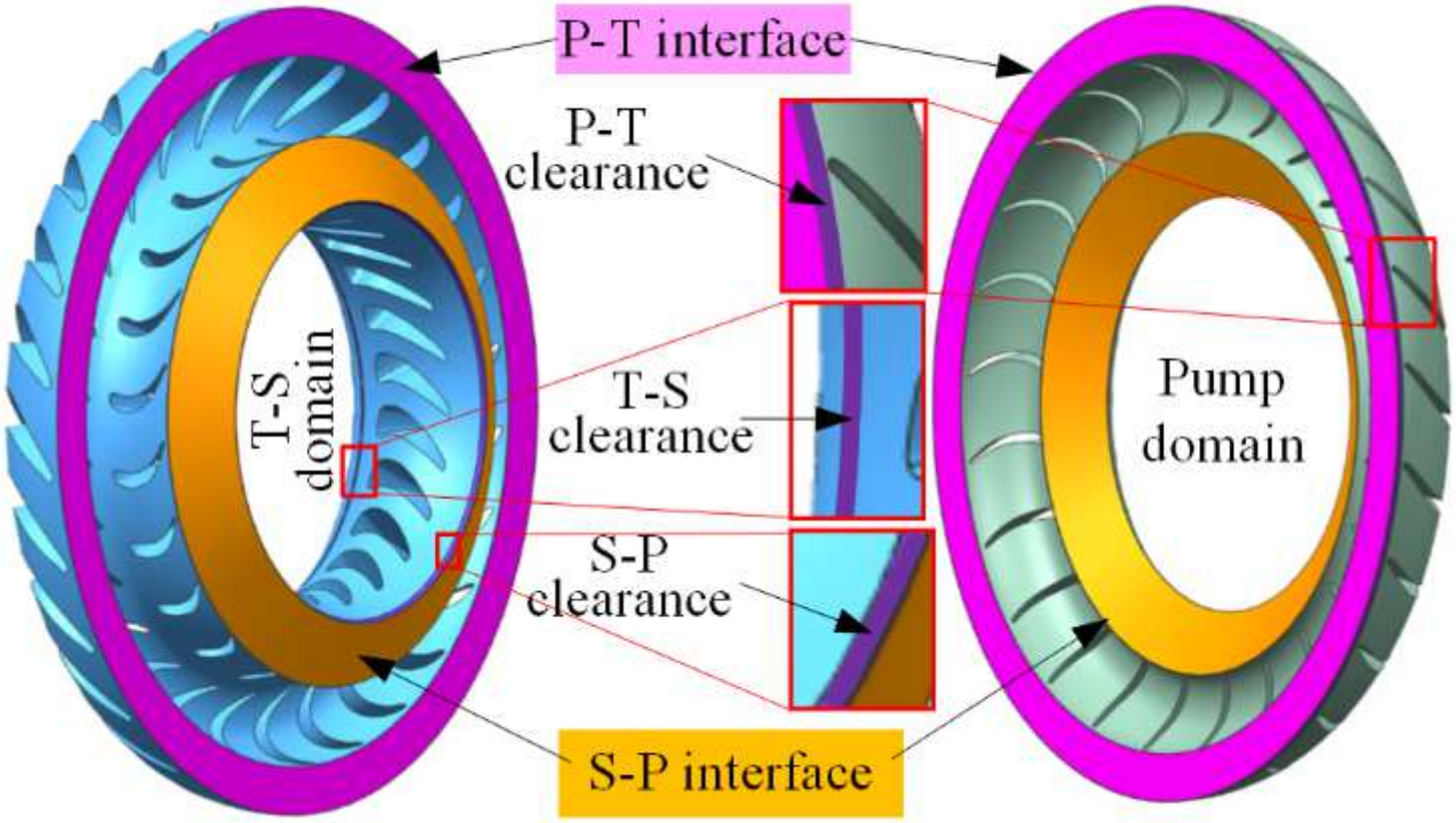

Figure 3

Full 3D fluid domains and boundaries

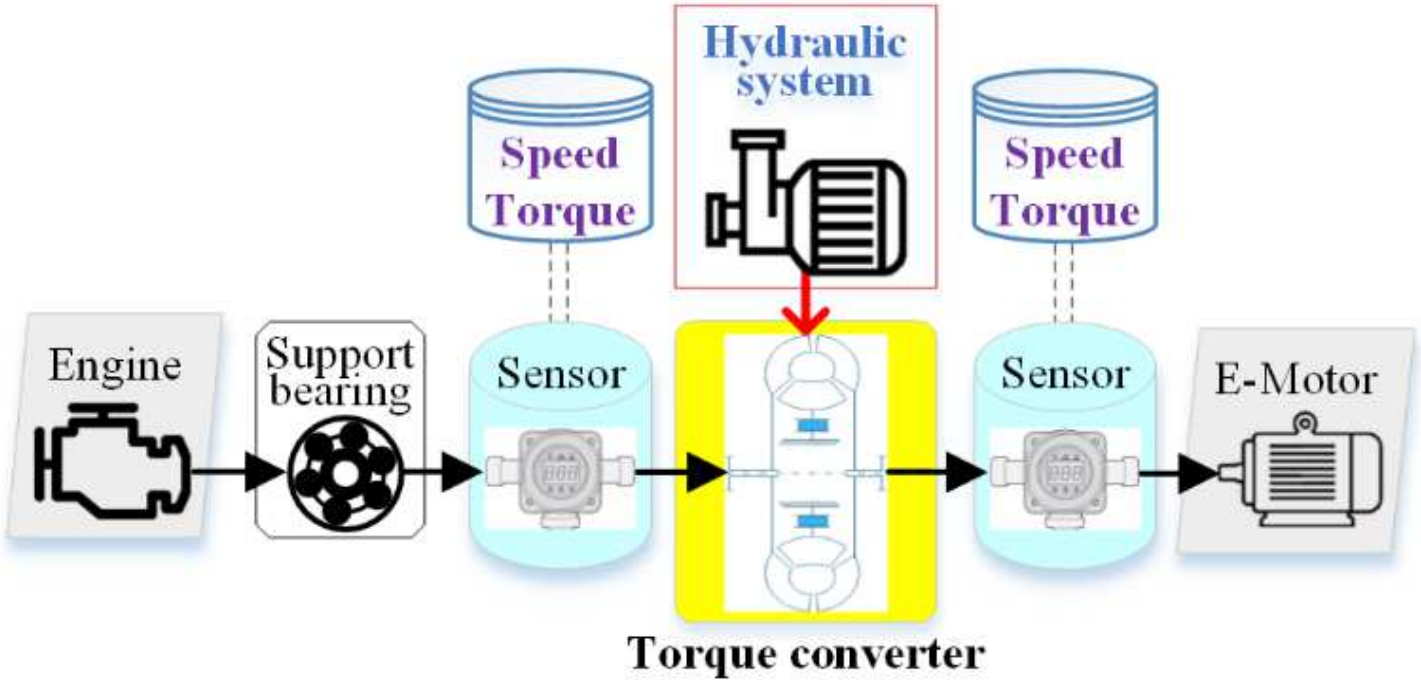

Figure 4

The schematic diagram of torque converter test cell

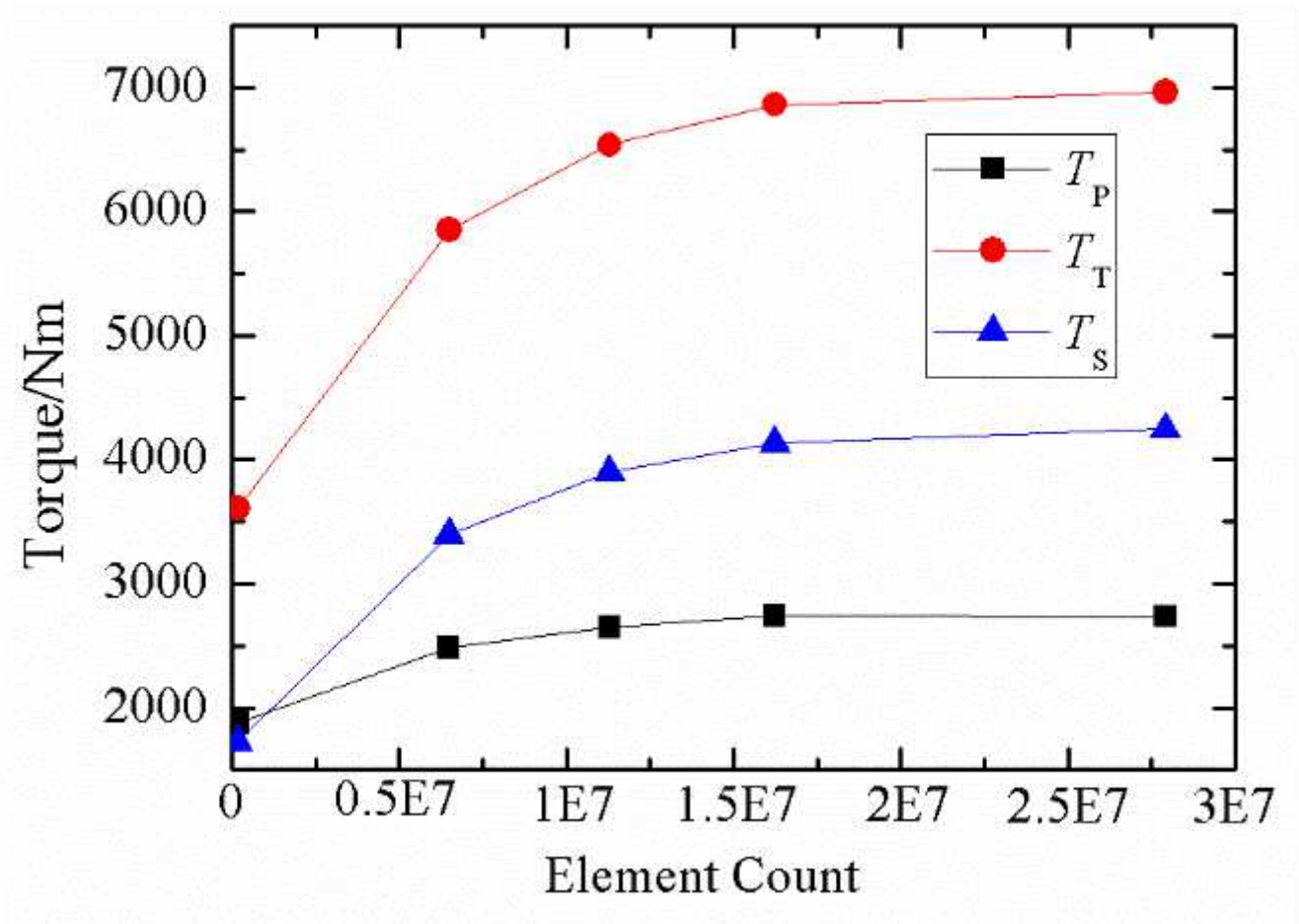

Figure 5

Predicted torque results under variant element density

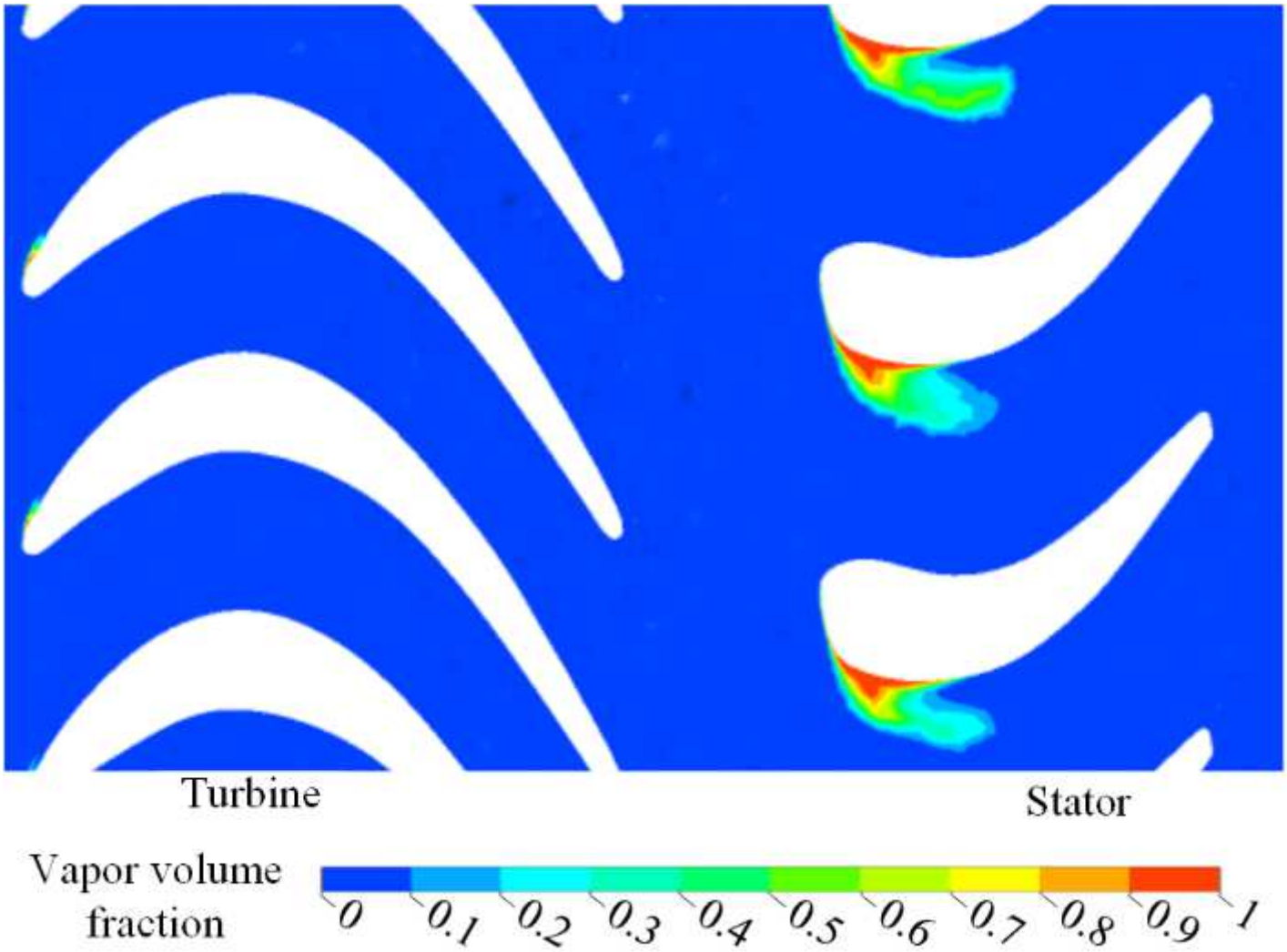

Figure 6

Vapour volume fraction distribution at the final time step for the base case.

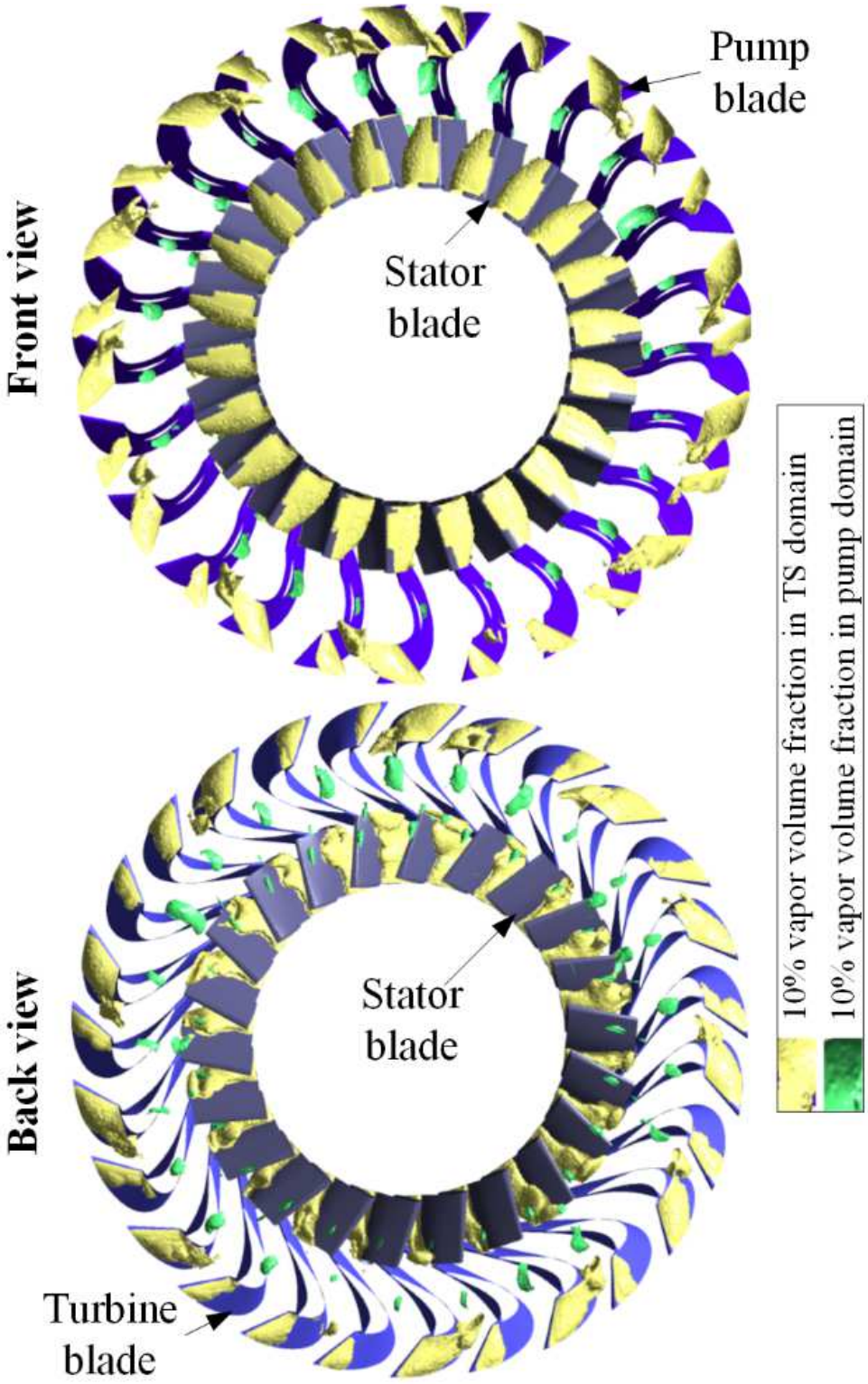

Figure 7

10% vapour volume fraction distribution in front view (looking at the stator leading edge) and back view (looking at the stator trailing edge)

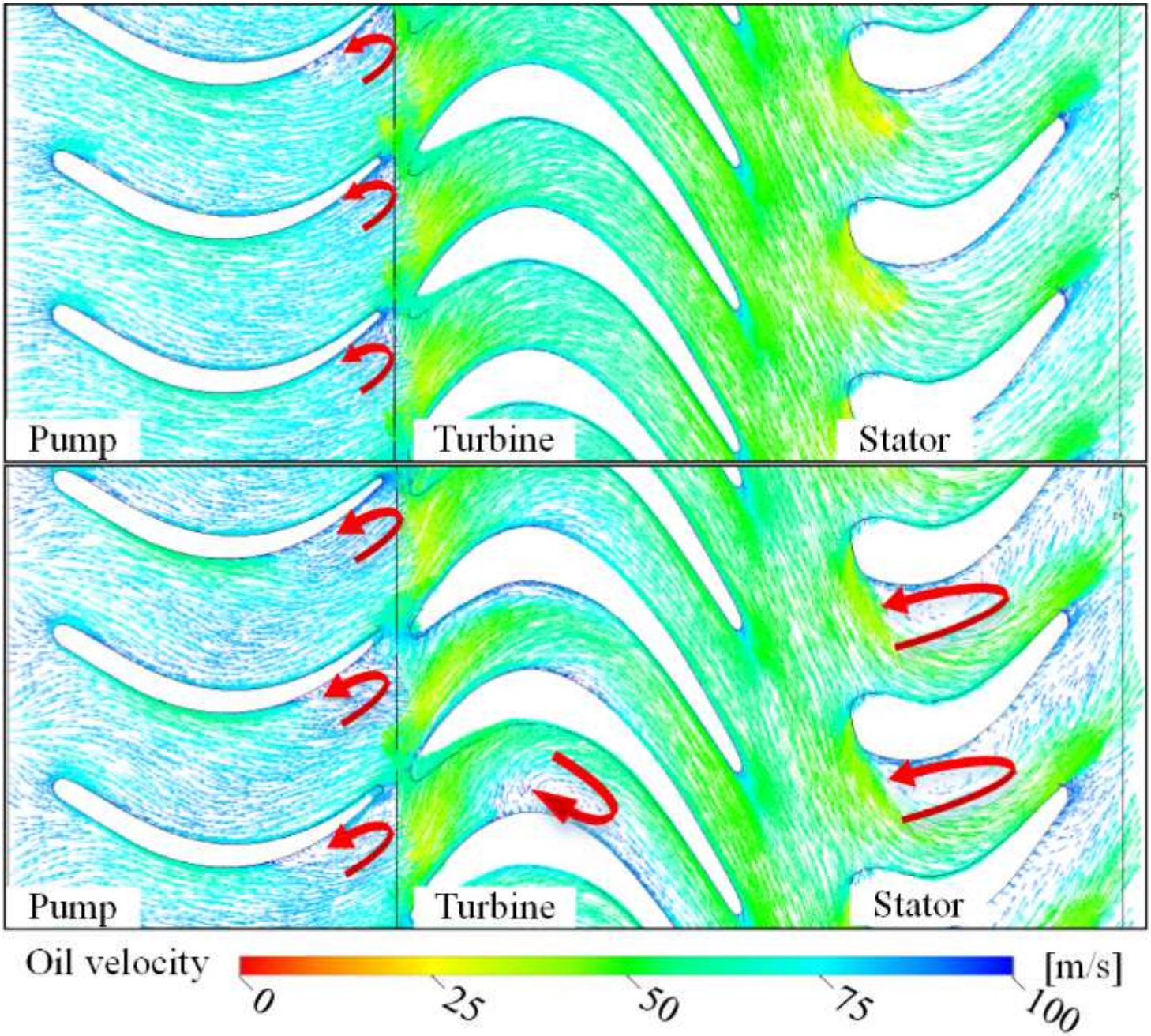

Figure 8

The oil velocity distribution derived from non-cavitation simulation (upper) and transient cavitation simulation at the final time step (lower). The reverse flow is indicated by arrow.

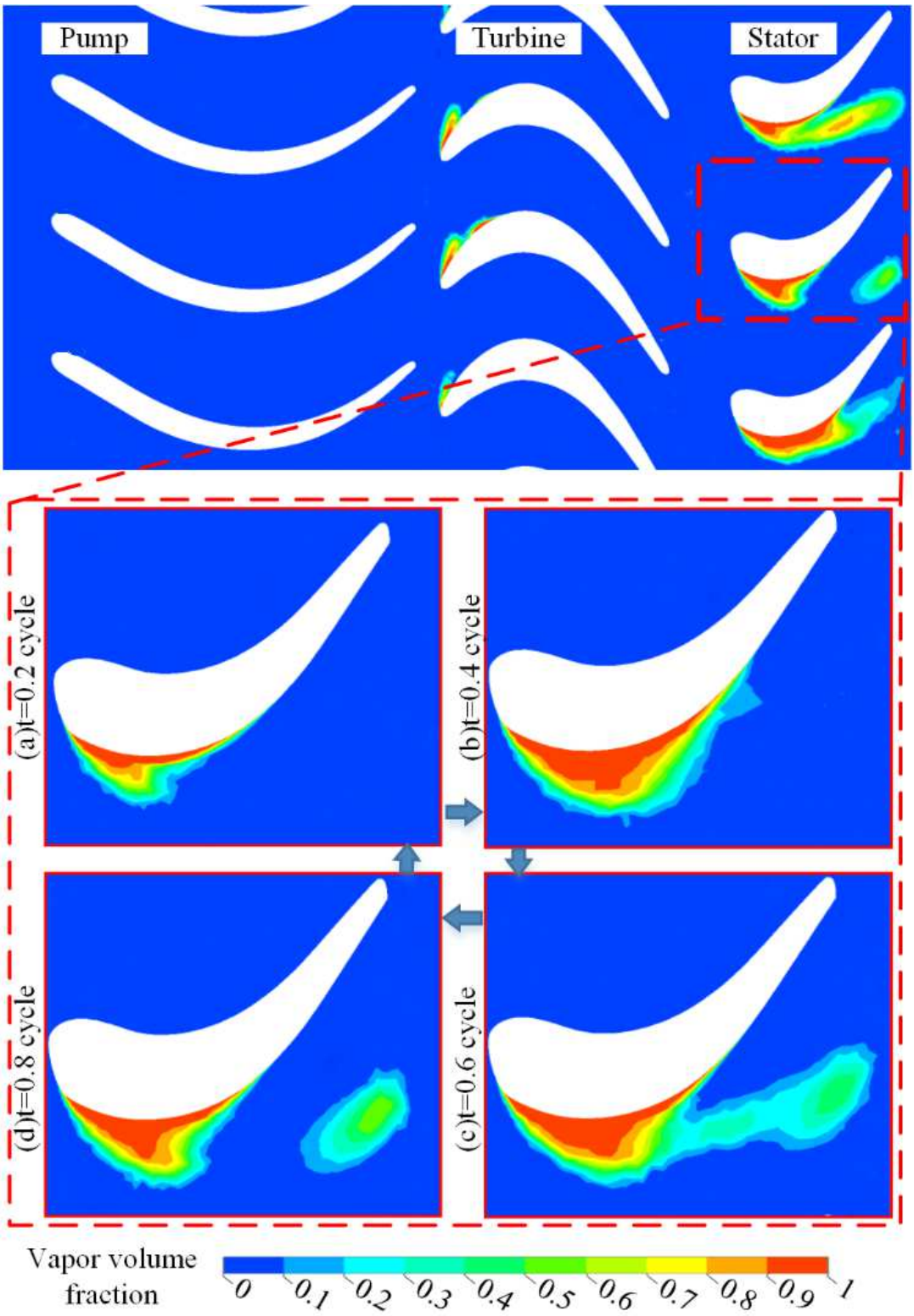

Figure 9

The transient cavitation process shown in the unfolded view

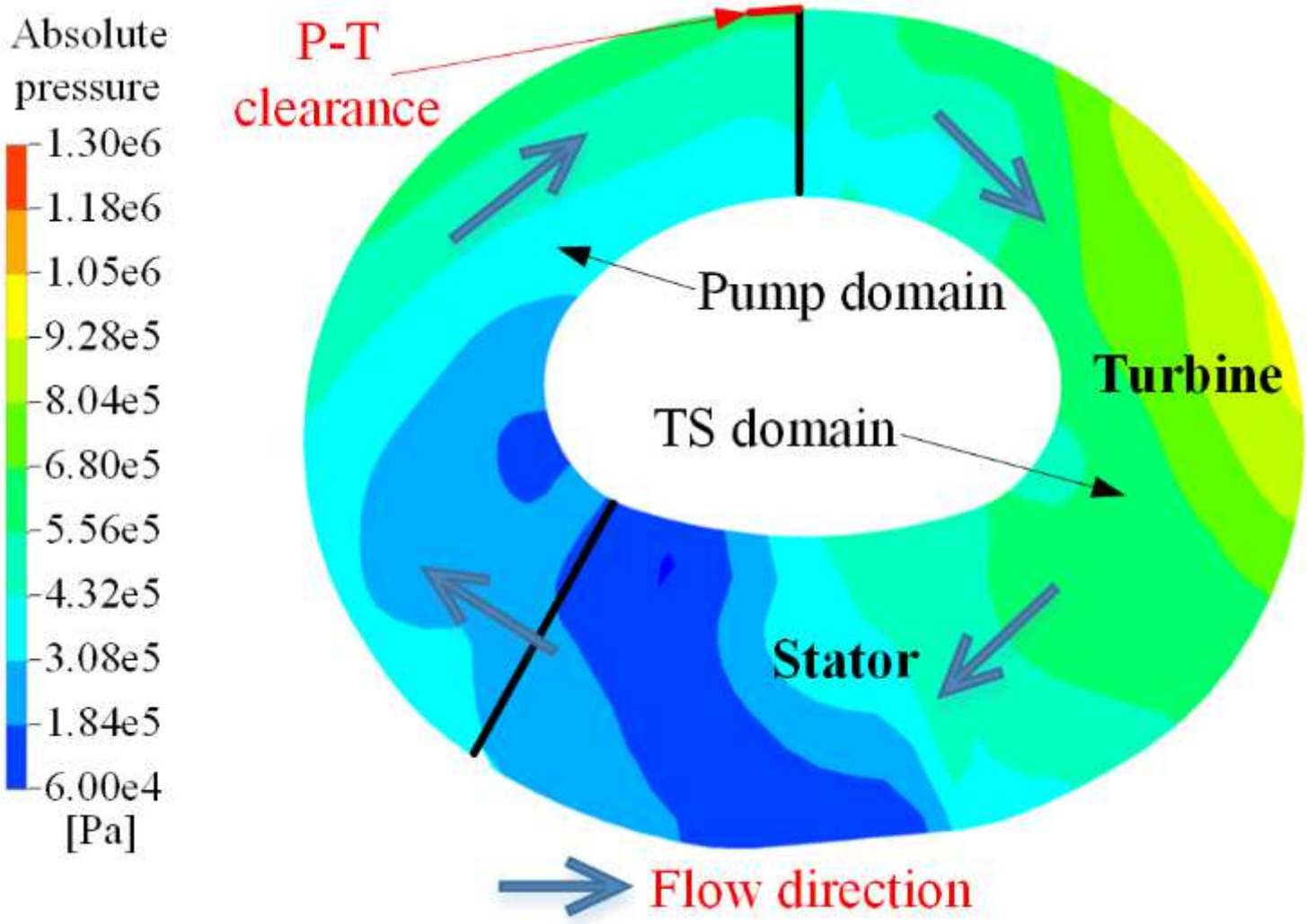

Figure 10

Meridionally averaged pressure distribution when the oil is charged from the P-T clearance. Charge pressure =0.6 MPa.

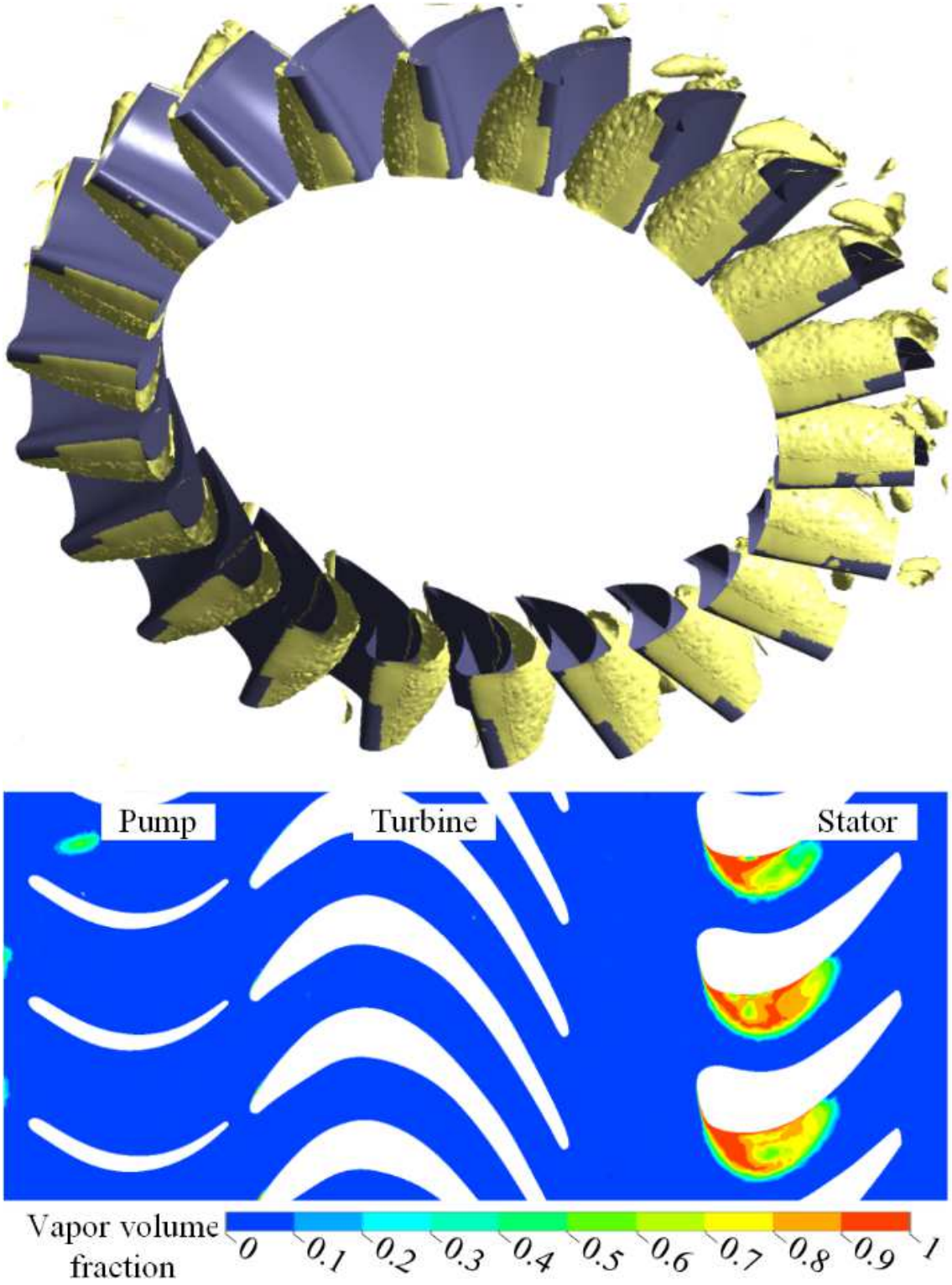

Figure 11

10% vapour volume fraction distribution (upper) and vapour volume fraction distribution in the unfolded view (lower) when the oil is charged from the P-T clearance. Charge pressure = 0.6 MPa

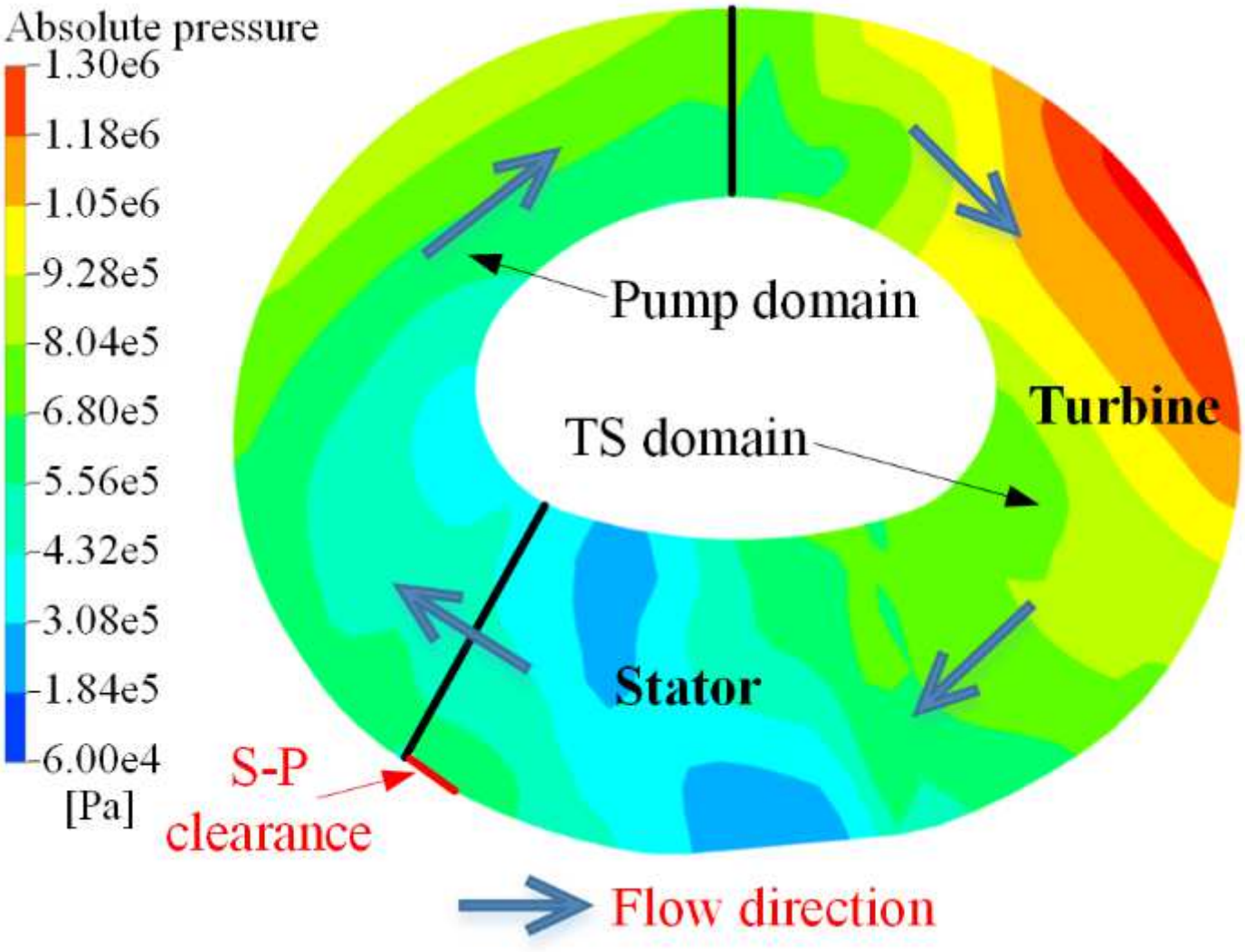

Figure 12

Meridionally averaged pressure distribution when the oil is charged from the S-P clearance. Charge pressure =0.6 MPa.

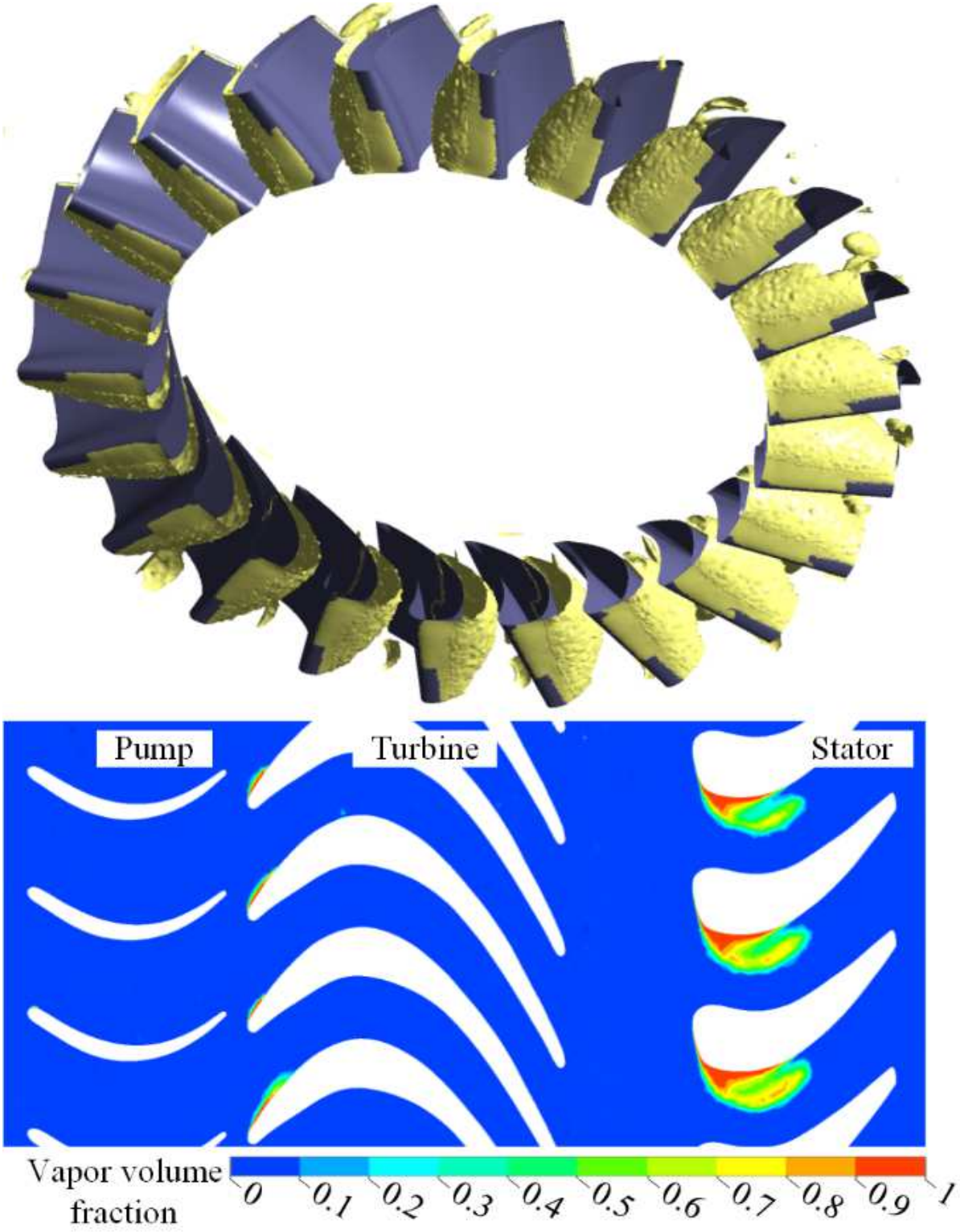

Figure 13

10% vapour volume fraction distribution (upper) and vapour volume fraction distribution in the unfolded view (lower) when the oil is charged from the S-P clearance. Charge pressure = 0.6 MPa

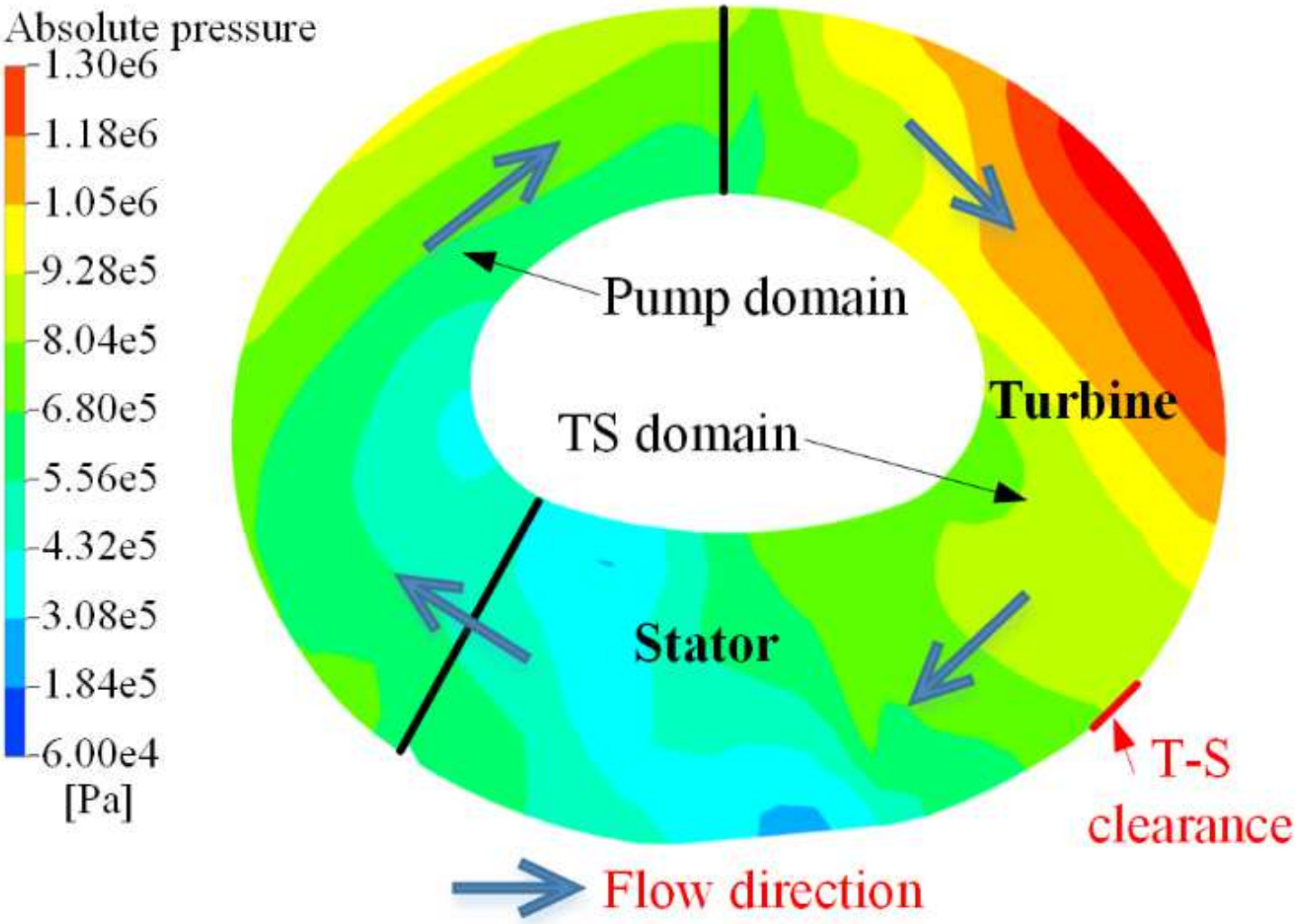

Figure 14

Meridionally averaged pressure distribution when the oil is charged from the T-S clearance. Charge pressure =0.6 MPa.

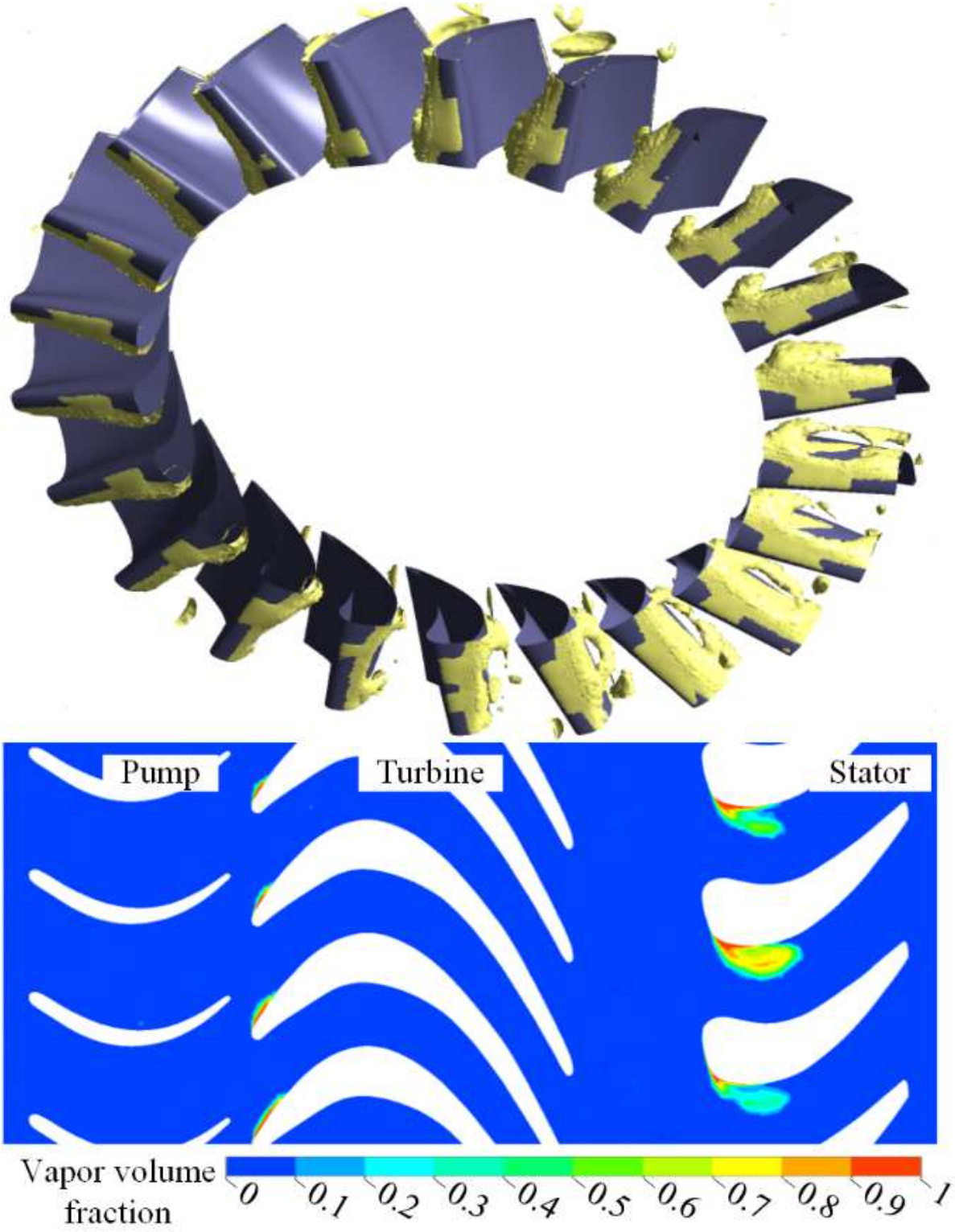

Figure 15

10% vapour volume fraction distribution (upper) and vapour volume fraction distribution in the unfolded view (lower) when the oil is charged from the T-S clearance. Charge pressure = 0.6 MPa

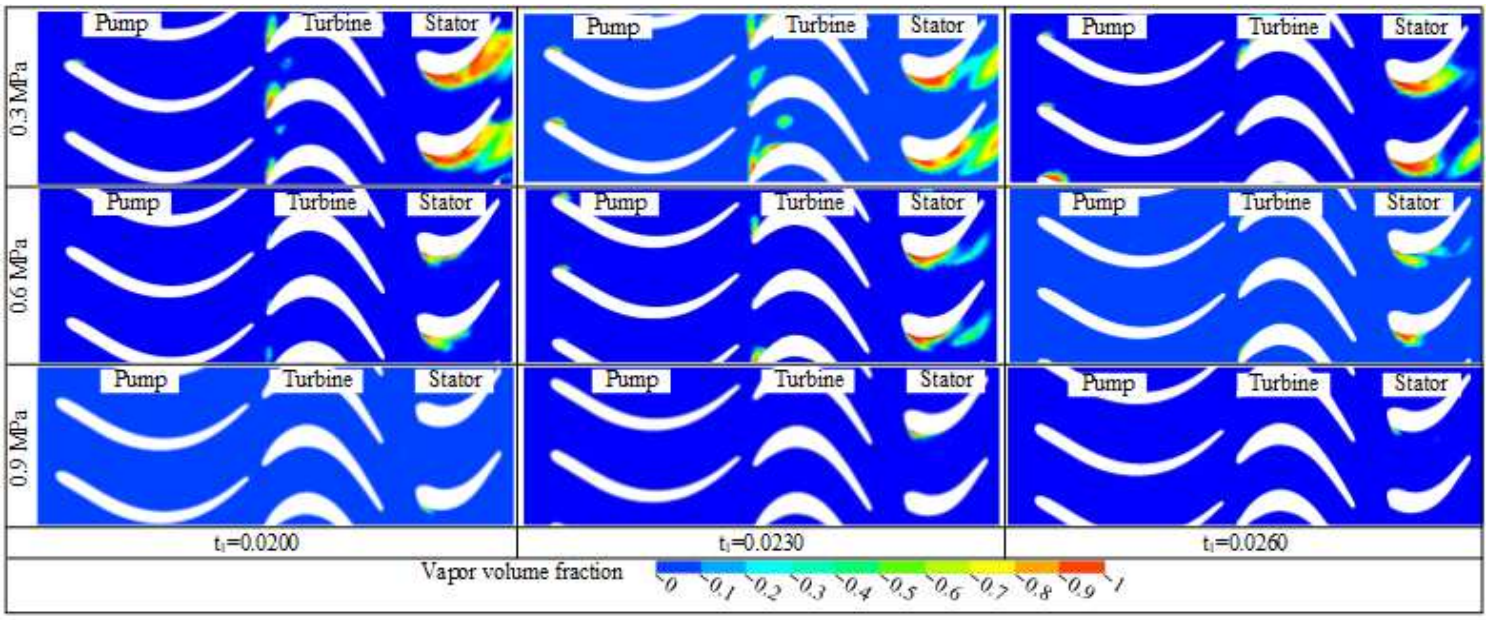

Figure 16

Vapour volume fraction distributions at different time steps over different charge pressures. The oil is supplied from the S-P clearance

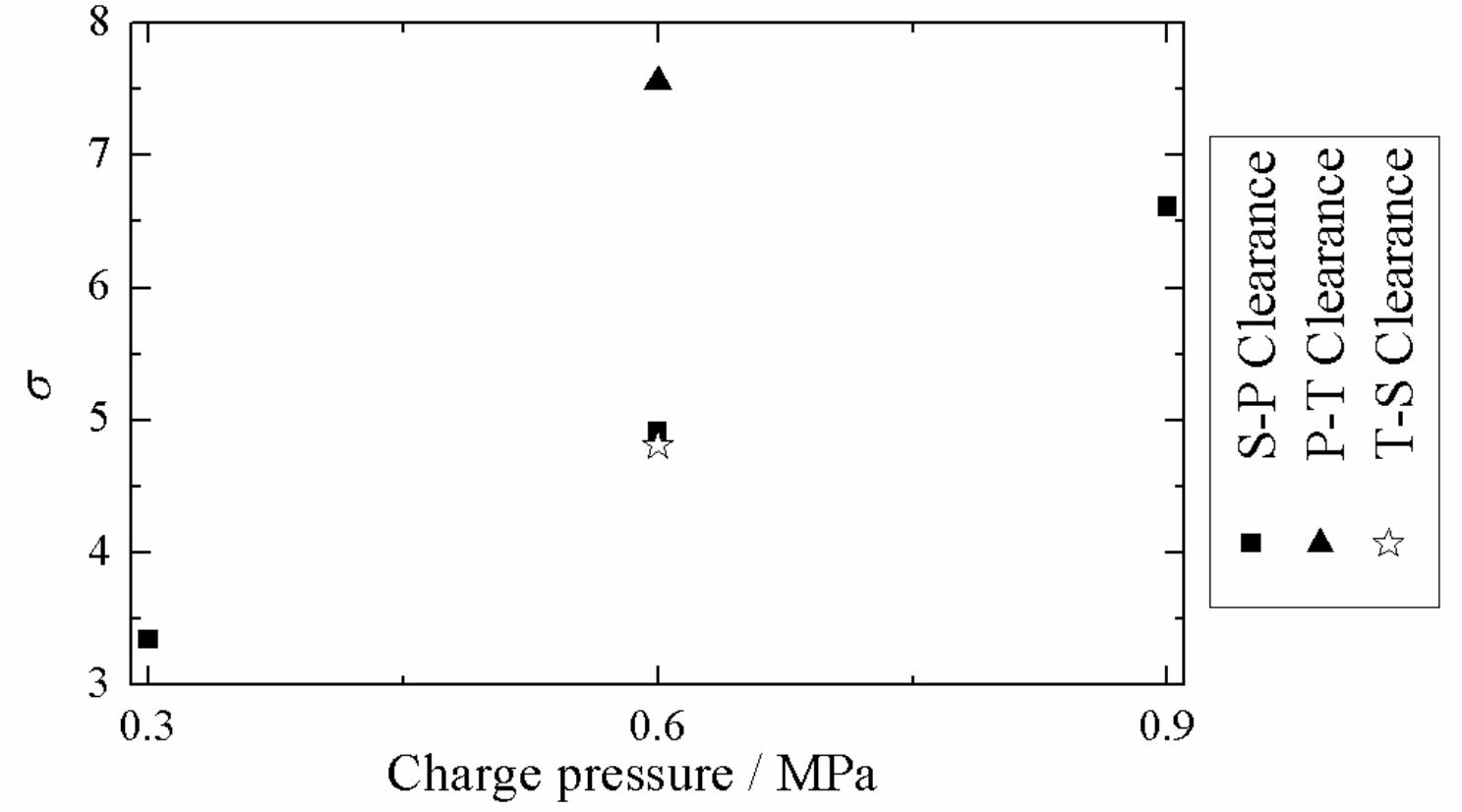

Figure 17

Cavitation numbers over various charge pressures and charge oil positions